Analysis of Leaky Wave Antennas Using the Matrix Pencil Method

Amardeep Singh

A Thesis
in
The Department
of
Electrical and Computer Engineering

Presented in Partial Fulfillment of the Requirements
for the Degree of Master of Applied Science
Concordia University
Montreal, Quebec, Canada

December 2014

CONCORDIA UNIVERSITY
SCHOOL OF GRADUATE STUDIES

This is to certify that the thesis prepared

By : Amardeep Singh

Entitled : "Analysis of Leaky Wave Antennas Using the Matrix Pencil Method"

and submitted in partial fulfillment of the requirements for the degree of

Master of Applied Science

complies with the regulations of this University and meets the accepted standards with respect to originality and quality.

Signed by the final examining committee :

_____ Chair
Dr. M. Z. Kabir

_____ Examiner, External
Dr. G. Gouw (MIE) To the Program

_____ Examiner
Dr. A. Kishk

_____ Supervisor
Dr. R. Paknys

Approved by _____
Dr. W. E. Lynch, Chair
Department of Electrical and Computer Engineering

_____ 20____

_____
Dr. Amir Asif, Dean
Faculty of Engineering and Computer Science

ABSTRACT

Analysis of Leaky Wave Antennas Using the Matrix Pencil Method

Amardeep Singh

The leaky-wave antenna (LWA) is a traveling wave antenna that uses a fast wave as the main radiating mechanism, where the fast wave is radiating continuously along the structure. Depending on the length of the antenna, some part of the fast wave gets reflected from the end and causes another beam in the opposite direction. The effects of the reflected fast wave on the radiation pattern can be analyzed if the reflection coefficient at the end of the antenna is known, which can be obtained from the complex amplitude and propagation constants associated with the fast waves. Even the radiation pattern of a LWA can be obtained using the reflection coefficient and propagation constants.

Closed top guiding structures, a dielectric slab waveguide, 2-D LWAs and 3-D LWAs are modeled in a commercial full wave MoM solver, FEKO. The near-field samples are calculated along the structure. For these types of structures, the total near field can be expressed as a sum of complex exponentials. The matrix pencil method (MPM) is a most accurate and efficient linear technique to approximate a function by a sum of complex exponentials. The exponential components from the total near field use the complex propagation constants inside the structure, which are calculated using the MPM. The MPM extracted amplitude and phase components are used to calculate the reflection coefficients of the structures and radiation patterns of the LWAs.

The accuracy of this approach is verified using various open and closed guiding structures in 2-D and 3-D, and by comparing the results with available numerical and experimental results.

Acknowledgements

I would like to express my deepest gratitude to my supervisor Prof. Robert Paknys for his academic and financial support. His guidance and encouragement made my thesis work a pleasant and extremely educational experience. I am grateful to him for giving me the opportunity to work with him in the field of leaky-wave antennas. I am thankful to Prof. Abdel Sebak and Prof. Yousef R. Shayan for their supervision and motivation during the courses in the early stages of my research.

Support from the National Science and Engineering Research Council (NSERC) is gratefully acknowledged. I am also thankful to the Graduate Program Coordinator Ms. Diane Moffat for her help and encouragement.

My sincere thanks to my parents and other family members for their support and sacrifices. I am also thankful to my friends and my colleagues for their support and motivations. Without their support I would have never been able to finish my thesis work.

Contents

List of Figures

List of Tables

List of Symbols and Abbreviations

EM	Electromagnetic
FEKO	*FEldberechnung fur Korper mit beliebiger Oberflache*, meaning Field Calculations for Bodies with Arbitrary shape
LWA	Leaky wave antenna
MPM	Matrix pencil method
MoM	Method of moments
PBC	Periodic boundary conditions
PEC	Perfect electric conductor
PMC	Perfect magnetic conductor
SDMoM	Spectral-domain periodic method of moments
SLL	Side-lobe level
$\mathbf{E}$	Electric field
$\mathbf{H}$	Magnetic field
$\mathbf{J}_s$	Equivalent electric surface current
$\mathbf{M}_s$	Equivalent magnetic surface current
α	Attenuation constant
β	Phase constant

c_0	Speed of light
ϵ_0	Free space permittivity
ϵ_r	Relative permittivity
η_0	Free space impedance
γ	Propagation constant
Γ	Reflection coefficient
k_d	Dielectric wavenumber
k_0	Free space wavenumber
μ_0	Free space permeability

Chapter 1

Introduction

The leaky-wave antenna (LWA) is a type of antenna which has been of interest for many years. A leaky wave antenna uses a traveling wave with a complex propagation constant as main radiating mechanism on a guiding structure and it operates differently from a slow wave or surface type of antenna, where the radiation mainly takes place at the end of the antenna [1]. The LWAs are capable of producing pencil beams or very narrow beams where the beamwidth is limited by the size of the antenna. Almost all the leaky wave antennas have a property that their beam scans as we change the frequency [2]. This could be a great property for the scanning applications, on the other hand it is a disadvantage for point-to-point communications, since the pattern bandwidth would be decreased along with the beamwidth. The pattern bandwidth is usually narrow, typically about 1% to 10% [3]. There is an advantage of simplicity in these type of antennas, since there is no need of any complicated feed network [4]. That is the reason behind their attraction for higher frequencies, like microwave and millimeter-wave.

Leaky-wave antennas can be divided into different categories, depending on their geometry and the principle of operation [2]. The first distinction that can be made is between a one-dimensional (1-D) leaky-wave antenna, a two-dimensional (2-D) LWA

and a 3-D LWA. Another classification is whether the structure is uniform/quasi-uniform or periodic. Furthermore, the distinction is if it is unidirectional or bidirectional. An antenna design is totally dependent on the application for which it is to be used. The various types of the LWAs are briefly summarized below.

A. *Uniform/Quasi-Uniform Unidirectional LWA*

The antenna is fed at one end and usually it is matched from the other end with an absorber or matched load to prevent reflected power. The aperture field has the form

$$H(x) = Ae^{-\gamma x}$$

where $\gamma = \alpha + j\beta$. The antenna radiates at an angle θ from the z-axis, where $\beta = k_0 \sin\theta_b$. Usually, the wave is a forward wave with a positive phase velocity ($\beta > 0$), which means the beam will be in the forward direction as shown in Fig. 1.1 (i.e., $0 < \theta < 90°$). On the other hand if $\beta < 0$, the beam will be in backward direction (i.e., $-90° < \theta < 0°$). The efficiency of this antenna is around 90% [2].

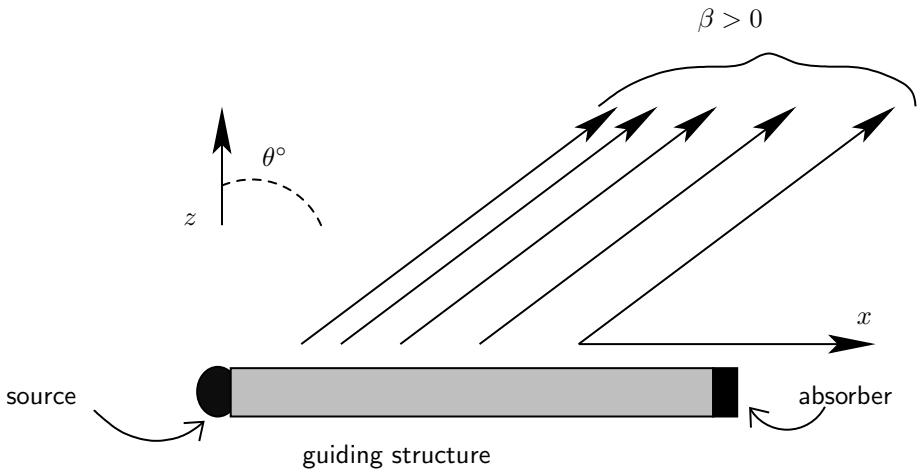

Figure 1.1: Unidirectional leaky-wave antenna with an absorber at the end, radiating in forward direction.

B. *Uniform/Quasi-Uniform Bidirectional LWA*

In this case, the structure is fed in the middle and absorbers or matched loads are placed at the both ends. The feed will excite the aperture field symmetrically in the form of

$$H(x) = Ae^{-\gamma|x|}.$$

The structure radiates two beams, in this case at angles $+\theta$ and $-\theta$ as shown in Fig. 1.2. The two conical beams will merge into a single beam at broadside (i.e., $\theta = 0°$) when $\beta < \alpha$ [2].

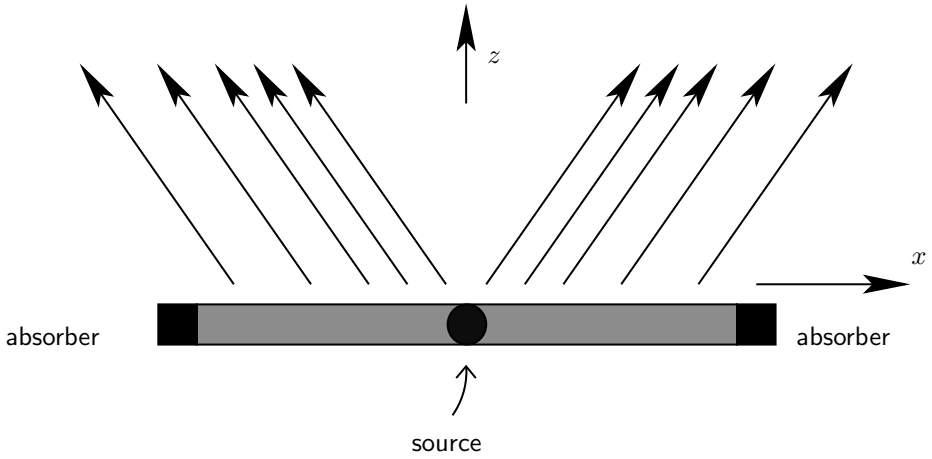

Figure 1.2: Bidirectional leaky-wave antenna with absorbers at each end, radiating in two directions.

C. *Periodic Unidirectional LWA*

This type of antenna is also fed at one end, with a load at the other end. The fundamental mode is a slow wave, but the $n = -1$ space harmonic will be the only one radiating. It may radiate in the forward (for $\beta_{-1} > 0$) or backward direction ($\beta_{-1} < 0$). Hence, this LWA can be used to create a beam pointing in either direction.

The beam angle of this LWA scans by increasing or decreasing the frequency. To make a scanable beam from backward endfire to forward endfire, so that

only the $n = -1$ harmonic radiates, the effective permittivity of the structure must be chosen so that $\epsilon^{eff} > 9$ [3].

D. *Periodic Bidirectional LWA*

This structure is fed in the middle, the same as in case B, and creates a bidirectional leaky wave. If the frequency of the operation is chosen exactly at the stop band so that $\beta_{-1} = 0$, the antenna will behave like a standing-wave antenna and will radiate at broadside, but it is not a traveling-wave structure anymore. The structure can radiate at broadside as a LWA by operating frequency slightly away from the broadside frequency (so that $\beta_{-1} > 0$ or $\beta_{-1} < 0$). The combination of two beams from each half of the antenna will produce a symmetrical broadside beam [3].

1.1 Literature review

The area of LWAs did not see a lot of development initially, but in the 1950s many different types of leaky-wave antennas were introduced, and some methods were developed for their analysis. To understand the research history of the LWAs and method of analysis, a brief literature review has been done in the following sections.

1.1.1 Development of leaky wave antennas

Initially, leaky-wave antennas were based on closed structures, mostly the waveguides, where long uniform slits were introduced into the waveguides to obtain the leakage and to allow them to radiate. The first known leaky-wave antenna was introduced by W. W. Hansen in 1940, which was a slitted rectangular waveguide [2] [5]. But, a strong perturbation on the fields was produced, because these slits cut across the current lines in the closed waveguides, which made it difficult to produce leaky waveguides with low leakage per unit length, and therefore narrow beams.

To overcome this difficulty, one method was proposed by Hines and Upson (mentioned in [2]); they replaced the long slit by a series of closely spaced holes, thereby avoiding cutting the current lines. This structure was known as a "holey waveguide," and it permitted the antenna to radiate much narrower beams.

A uniform 2D leaky-wave antenna was investigated by Alexopoulos and Jackson in the 1980s [6], consisting of a dielectric superstrate layer over a substrate layer. The analysis of this type of structure as a leaky-wave antenna was also done by Jackson and Oliner in the late 1980s and early 1990s [6] [7]. They showed the term "*leaky wave*" can be used to describe the resonance gain effect.

Later, two dimensional leaky-wave antennas using periodic partially reflecting screens were examined in more detail by Feresidis and Vardaxoglou using quasi-uniform partially reflective screens consisting of various elements including metal dipoles and rectangular patches [8]. Two dimensional uniform LWAs were designed and analyzed using the metal patches and slots on the top of the antenna by Zhao and Yang during 2003 to 2005 [9].

In most recent years the developments have been towards planar LWAs. These are low profile antennas which are easy to manufacture. The reason behind these developments is partly due to the interest in metamaterials. Some recently developed LWA types (as discussed in [3]) are:

A. Endfire Substrate Integrated Waveguide LWA.

B. Quarter-Wave Transformer LWA.

C. Composite Right/Left-Handed LWA.

D. Phase-Reversal LWA.

E. Ferrite LWA.

F. Conformal LWA.

1.1.2 Development of the matrix pencil analysis

The problem of approximations of a function by a sum of complex exponentials is at least two centuries old [10]. In more recent times, applications of these approximations have been found in other areas of electromagnetics: for example, the efficient evaluation of the Sommerfeld integrals and in antenna-pattern synthesis [10]. The term "pencil" originated with Gantmacher in 1960 [11]. There are two popular linear methods, "polynomial method" (also known as Prony's method) and "matrix pencil method" (also known as generalized pencil-of-function GPOF). The polynomial method is a two step process and the matrix pencil method is a one step process. The MPM solves a generalized eigenvalue problem to find the unknown complex propagation constants γ_m for a given signal that is expressed as

$$S(x) = \sum C_m e^{-\gamma_m x}.$$

Sarkar in [10] confirmed that of all linear techniques to approximate a function by a sum of complex exponentials, the matrix pencil method (MPM) provides a smaller variance of the parameters in the presence of noise. MPM is more efficient than the old pencil-of-function (POF) method, even though both start with same philosophy. Hua in [12] presented that when the number of samples more than 50, the MPM is computationally more efficient than other linear methods.

Sarkar et al. in [13] used the MPM to determine the propagation characteristics of printed circuits. The microstrip structures were solved by using the MoM and then the MPM was used to decompose the currents along the feed into forward and backward traveling waves. They used this approach to predict the input parameters of LWAs and the scattering parameters of printed circuits. Menzel's leaky-wave antenna [13] was analyzed by them using the MPM. They were able to decompose the current along the microstrip into various modes with an overall good agreement with theory,

and an error of less than 2.5%.

In general, the MPM can be used effectively to estimate the one dimensional spectral frequencies. Altman et al. in [14] used the MPM or GPOF to represent the decomposition of the induced currents on large scatterers into different current components. Nallo, Mesa and Jackson in [15] used the GPOF to study the correlation between the leaky-mode current and the total current. They decomposed the total current on the strip into the exponential waves. The amplitude and propagation constant of the these waves were compared with the constants of leaky mode with a good agreement. Chen et al. in [16] applied the MPM to the surface current and extracted the space harmonics of the modes propagating in the periodic guiding structure and combined the MPM analysis with another method (Brillouin diagram) to discover the unknown modes in the structure.

Ozturk in [17] used the MPM to extract the parameters as a sum of complex exponentials for vertex diffraction. The current density was decomposed into different current components those were diffracted from the different edges and corners of a scatterer. In [18], Ozturk and Paknys used the MPM to calculate the complex propagation constant between rows of conducting cylinders. They verified the accuracy of this approach by using numerical and experimental results.

These studies clearly described the efficiency of the MPM in the approximation of a function by a sum of complex exponentials, as well as the validity of the decomposition of the MoM currents into various modes.

1.2 Objective

This thesis is concerned with the analysis of the characteristics of some leaky-wave antennas. The main focus of this analysis is to calculate the reflection coefficient (Γ) from the propagation constants and amplitude coefficients extracted by using the ma-

trix pencil method (MPM) and the least-squares method respectively. It is expected that the extracted components can be used to calculate the reflection coefficient at the end of the structure, which then can be used to obtain the radiation pattern of the antenna. It is desired that the MPM extracted propagation constants and amplitude coefficients should be enough to analyze LWAs and waveguides.

1.3 Basic assumptions and considerations

In this work, a commercial EM software FEKO is used to design and solve for the field on all of the structures. It uses the method of moments (MoM) to solve for currents and to calculate the near-fields [19]. The MoM near-field samples are considered as the sum of complex exponentials. In this thesis, the complex exponentials are calculated using the MPM and the complex amplitude coefficients are extracted using the least-squares method, but the term "MPM extractions" is used for both extractions together. In this thesis, the periodic boundary conditions (PBC) are used when needed to make a 2-D geometry infinite in the required axis. Plane wave excitation is used for the two dimensional structure because this the only option in FEKO for 2-D structures, so just receiving antennas can be analyzed. In 3-D problems, an array of magnetic dipoles is used near the origin inside the structure to approximate a uniform line source of finite length. There are many other sources available for 3-D problems in FEKO, which means transmitting antennas can be analyzed.

1.4 Thesis outline

This thesis is organized as follows: Chapter 2 explains the brief theory behind the matrix pencil method (MPM) approach. The steps of calculation are explained with the brief description of the requirements to make a computer program that uses the MPM and least-squares method. A test problem is solved using the computer

program to verify its accuracy. Chapter 3 presents the use of the MPM to extract the field components for closed-top guided structures. The structures are modeled and solved in a MoM solver (FEKO) to obtain the field samples, then those field samples are used to extract the propagation constant of the structure. The MPM extracted components are then used to calculate the reflection coefficient (Γ) at the end of the structures and the results are compared with the theoretical results. Chapter 4 starts with the design principles of a 2-D unidirectional periodic LWA, which is then modeled and solved with the MoM to obtain the field samples. Then using the MPM the behavior of the leaky waves are analyzed. The idea of using extracted components to plot the radiation pattern starts with the modification of the free-space radiation integral and the results are compared with known theoretical results. The effects of edge diffractions are also discussed. The procedure of calculating the reflection coefficient from the MPM extracted fast-wave components is then explained and used. Chapter 5 investigates the 3-D unidirectional periodic LWAs using the MPM. The space harmonics are extracted by using the MPM and the MoM field samples. The results are compared with the theoretical Floquet harmonics. The radiation pattern is plotted and the effects of the space-waves are also discussed. Then, the extracted components are used to calculate the reflection coefficient of the LWAs. The effects of strip length on the radiation behavior of the 3-D LWA are presented. Finally, Chapter 6 presents the conclusions and some suggestions for the future work.

Chapter 2

Matrix Pencil Method

2.1 Introduction

The matrix pencil method (MPM) or generalized pencil-of-function (GPOF) method is a very useful linear technique for the approximation of a function by a sum of complex exponentials. The polynomial method (also known as Prony's method) is another popular linear technique to solve this type of problem, but it has been found that the MPM is more efficient in the presence of noise. Also, the polynomial method is a two-step process to find the poles, where the first step solves the matrix equation and the second step involves approximating the root of the polynomial, on the other hand the MPM is a one-step process and it approximates the poles by solving a generalized eigenvalue problem. In more recent times, the utility MPM has been found in many areas of electromagnetics.

In this chapter, the utilization of the MPM is explained. In Section 2.2, the methodology behind this method is explained with a brief description of the implementation of the MPM using a computer program. In Section 2.2.1, the MPM program is tested by solving a test problem, where we already know the exact values of all the components.

2.2 Component extraction methodology

If we assume a very general short circuited waveguide structure as shown in Fig. 2.1, the total field sampled at constant intervals Δx inside the structure can be expressed as the sum of the complex exponentials

$$E_z(n\Delta x) = \sum_{m=1}^{M} C_m e^{-\gamma_m n\Delta x},\ n = 1, 2, \cdots, N \tag{2.1}$$

where N represents the number of samples, M is the number of components and C_m and γ_m are the complex amplitude and phase factors for m^{th} components. From (2.1),

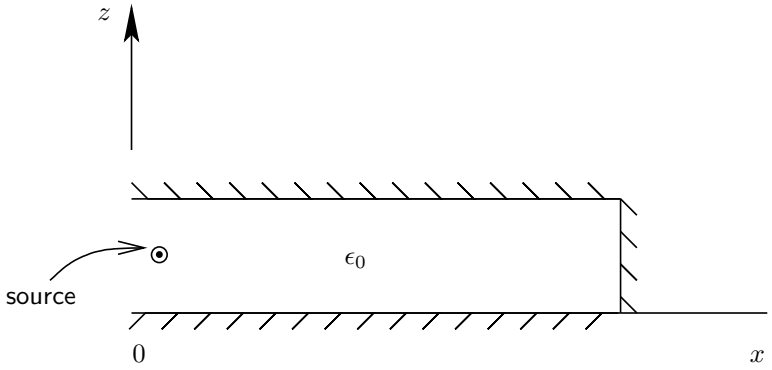

Figure 2.1: Parallel plate waveguide in x-z plane with a perfect conducting short circuit at the end.

the total field at the n^{th} sampling point can be written as

$$E_z(x_n) = \sum_{m=1}^{M} C_m z_m^n,\ n = 1, 2, \cdots, N \tag{2.2}$$

where $z_m = e^{-\gamma_m \Delta x}$ and $x_n = x_o + n\Delta x$. Following the procedure for the MPM extractions as described in [18], [20] and elsewhere, two matrices of field samples can be defined as

$$\mathbf{G_1} = (\bar{y}_1 \quad \bar{y}_2 \quad \bar{y}_3 \quad \cdots \quad \bar{y}_P) \tag{2.3}$$

$$\mathbf{G_2} = (\bar{y}_2 \quad \bar{y}_3 \quad \bar{y}_4 \quad \cdots \quad \bar{y}_{P+1}) \tag{2.4}$$

with

$$\bar{y}_i = (E_i \quad E_{i+1} \quad E_{i+2} \quad \cdots \quad E_{(N-P)+i-1})^T \tag{2.5}$$

where $\mathbf{G_1}$ and $\mathbf{G_2}$ are $(N-P) \times P$ matrices and P is the pencil parameter used to obtain column vectors by windowing the field samples with the window length $N-P$. P is chosen such that $M \leq P \leq N-P$. Hua and Sarkar in [21] explained that for a pencil parameter $P = M$ this method is same as Prony's method and when $P = N/2$ the MPM or GPOF is most efficient in the presence of noise.

By using (2.3) and (2.4), it can be shown that the poles z_m are the eigenvalues of the generalized eigenvalue problem

$$\mathbf{G_2}\bar{e}_m = z_m \mathbf{G_1}\bar{e}_m \tag{2.6}$$

where $\bar{e}_m$ are the generalized eigenvectors of the pencil $(\mathbf{G_2} - z_m\mathbf{G_1})$. Now, using singular value decomposition [22] for $\mathbf{G_1}$, it can be expressed as

$$\mathbf{G_1} = \mathbf{U}\mathbf{D}\mathbf{V^H} \tag{2.7}$$

where $\mathbf{U}$ and $\mathbf{V}^H$ are unitary matrices associated with left and right singular vectors respectively. Here, H denotes the conjugate transpose and $\mathbf{D}$ is a diagonal matrix with singular values of $\mathbf{G_1}$ on the diagonal in descending order. $\mathbf{U}, \mathbf{D}$ and $\mathbf{V}^H$ are $(N-P)\times(N-P)$, $(N-P)\times P$ and $P \times P$ respectively. The largest M singular values and the associated left and right singular vectors are chosen in (2.7). By multiplying left side of (2.6) by $\mathbf{V}\mathbf{V^H}$ and substituting in (2.7) it reduces to a square matrix

$$\mathbf{D}^{-1}_{(M\times M)}\mathbf{U}^{\mathbf{H}}_{(M\times N-P)}\mathbf{G_2}_{(N-P\times P)}\mathbf{V}_{(P\times M)}\mathbf{V^H}\bar{e}_m = z_m\mathbf{V^H}\bar{e}_m. \tag{2.8}$$

Therefore, z_m are simply the eigenvalues of the $M \times M$ matrix in (2.8). Once z_m are

calculated, the complex propagation factors can be calculated by using

$$\gamma_m = -\frac{\ln z_m}{\Delta x},\ m = 1, 2, \cdots, M. \tag{2.9}$$

The complex amplitude components C_m can be obtained by using z_m in (2.2) and solving an overdetermined linear system of equations by using a least-squares fit. Once the unknown complex amplitude and phase factors are obtained, the original near-field behavior can be reconstructed. It should be noted that the MPM is only required to approximate the propagation constants, if we already know the propagation constants γ_m then the C_m can be approximated using the least-squares method and the MPM is not required.

FORTRAN subroutines: To solve the exponential poles using the matrix pencil approach, a FORTRAN program is developed and used. The program uses various subroutine packages that are provided by Dongarra in [23]. Each primary subroutine is used for its dedicated purpose. To calculate the singular value decomposition (SVD) in (2.7), primary subroutine "`CGESVD`" is used. Then to find eigenvalues in (2.8), subroutine "`CGEEVX`" is used. The propagation constants γ_m are calculated using (2.9). Eventually, subroutine "`CGELS`" is used to solve the overdetermined system of linear equations by using a least-squares fit to approximate the associated amplitude components C_m. There are many other secondary subroutines required to support the primary subroutines. So, all the primary and secondary subroutines are required to develop a program that does the MPM extractions as explained above.

2.2.1 Verification of the computer program

It is desired that the computer program should work as expected from the theory of the MPM. In order to verify the correctness of the program a test problem is introduced, where we already know the components. Those are used to generate the

field samples by using (2.1). Considering the sampling interval $\Delta x = 0.001$ (which in EM problems will be selected w.r.t. the wavelength), the field samples $N = 300$ are generated by using the input components from Table 2.1. By using resultant $E_z(n\Delta x)$ as an input to the MPM program, the components are extracted from the field samples by using $N = 150$, $M = 4$ and $\Delta x = 0.001$.

Exponential components (γ_m)	Input components	Output components (MPM extracted)
γ_1	$1.500 + j20.00$	$1.502 + j20.00$
γ_2	$-1.500 - j20.00$	$-1.502 - j19.99$
γ_3	$2.400 - j40.00$	$2.398 - j40.00$
γ_4	$-2.400 + j40.00$	$-2.400 + j40.00$
Amplitude components (C_m)	**Input components**	**Output components (MPM extracted)**
C_1	$2.200 + j3.400$	$2.200 + j3.400$
C_2	$1.500 - j2.500$	$1.499 - j2.500$
C_3	$4.200 + j3.500$	$4.199 + j3.499$
C_4	$3.200 - j2.600$	$3.199 - j2.599$

Table 2.1: Input and output components for the test problem to verify the accuracy of the computer program.

It can be seen in Table 2.1 that the MPM extracted components are in excellent agreement with the input components. For the matrix pencil extractions the number of samples $N = 150$ was used. It can be chosen as larger or smaller, depending on the complexity of the problem. So, this program is used throughout this research to calculate the unknown amplitudes C_m and exponential components γ_m.

In electromagnetic problems, the field samples from the MoM can be used as input samples for MPM computer program. It should be noted that the sampling region and interval for the MoM field should be large enough, so that all the wave characteristics can be captured. The sampling interval Δx will be chosen between $\lambda_g/40$ to $\lambda_g/20$, where λ_g is the wavelength along the guiding structure.

2.3 Summary

In this chapter, the theory of the matrix pencil method (MPM) was explained. The procedure of utilizing the MPM to extract the unknown components from a set of field samples was described. Various subroutines were described. They are required to make a computer program that calculates the unknown amplitudes C_m and exponential components γ_m by using the least-squares method and the MPM respectively.

Finally, the computer program was tested using some known components. It was found that the program successfully extracts the exact components from the samples.

Chapter 3

Guiding Structures Analysis

3.1 Introduction

The guiding structures guide the electromagnetic waves in a particular direction. There are different types of the guiding structures, the mode of the wave traveling inside depends upon the structure and the frequency of operation. Usually the waves inside can be described as "zig-zags" between the walls of the waveguide. Actually, the propagation inside the structure depends on the propagation constant. If we know the propagation constant of a guiding structure, we can analyze the field behavior and the wave propagation inside the structure.

The outline of this chapter is as follows. In Section 3.2, the propagation constants of various closed-top guiding structures and a dielectric slab waveguide are analyzed. Firstly, the MoM is used to calculate the near-field samples inside the structures. The matrix pencil method (MPM) is used to extract the propagation constants from those MoM samples. Then the extracted components are successfully used to reconstruct the original field. Finally, the extracted propagation constants and amplitude coefficients are used to calculate the reflection coefficient at the end of the structure.

3.2 Propagation constants analysis

The complex propagation constant γ, is a measure of the change undergone by an electromagnetic wave as it propagates in the given structure in the guiding direction. The propagation constant is a complex quantity which has a real as well as an imaginary part (i.e., $\gamma = \alpha + j\beta$). Where α is the *attenuation constant* and β is the *phase constant*. The attenuation constant α represents the rate of decay along the path traveled by the wave and is measured in *Nepers per meter*. The phase constant β represents the change in the phase along the path traveled by the wave and is measured in *radians per meter*. If we assume that, inside the guiding structure a wave with a magnetic field H_y travels along the x-axis and has an incident as well as a reflected part, it can be written as

$$H_y(x) = C_1 e^{-\gamma x} + C_2 e^{+\gamma x}. \tag{3.1}$$

The $+x$ traveling wave is represented by the propagation factor of form $e^{-\gamma x}$ and the $-x$ traveling wave is represented by the propagation factor $e^{+\gamma x}$. C_1 and C_2 are amplitude coefficients associated with the right and left traveling waves respectively. The positive traveling phase factor can be written as

$$e^{-\gamma x} = e^{-\alpha x} e^{-j\beta x}, \tag{3.2}$$

where the $\alpha > 0$ means the wave is decaying as it travels along $+x$. This equation can be represented in the time domain as,

$$e^{-\alpha x} e^{-j\beta x} \leftrightarrow e^{-\alpha x} \cos(\omega t - \beta x). \tag{3.3}$$

This represents a wave traveling in the $+x$ direction with a phase velocity $v_p = \omega/\beta$ and a wavelength $\lambda = 2\pi/\beta$ with an exponential damping factor. If we remove the

loss from the structure, we will have $\gamma = jk_d$, which means $\alpha = 0$, $\beta = k_d$. There is no attenuation constant for the lossless waveguide and the phase constant β is the same as the wavenumber k_d for that medium.

In order to extract the complex propagation constant, we will first calculate the H_y-field inside of the structure; this can be accomplished by using the MoM. Then by using these MoM samples as data for the MPM, the complex amplitude and phase factors associated with this field will be extracted using the MPM.

3.2.1 Air filled, short circuited parallel plate waveguide

In order to verify the accuracy of the MPM, it is required to first use this method to extract the propagation constants for the structures for which we already know the γ_m. A very easy and common structure where we know the exact answers is this, an "*air filled, short circuited parallel plate wave guide.*" It is infinite in the y direction as shown in Fig. 3.1, which means this is a 2D problem. A vertically polarized incident plane wave at $\theta = -90°$ is used to excite the structure . In this problem $f = 27$ GHz, $\ell = 47.5$ mm and $h = 2.5$ mm.

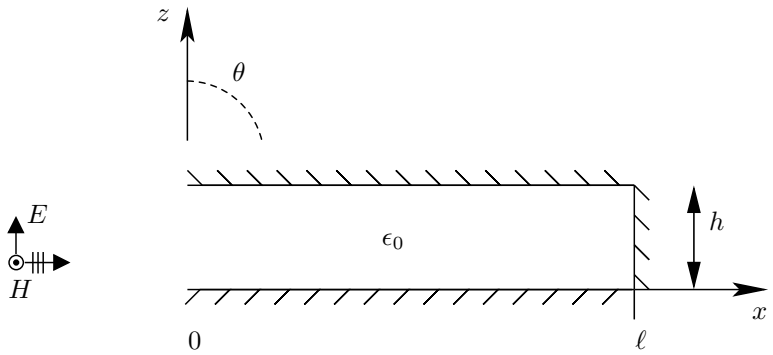

Figure 3.1: Air filled parallel plate waveguide with a short circuit at the end.

According to the theory, for a structure like this where there are no losses we have exact results, i.e., this is a TEM wave with the attenuation constant $\alpha = 0$ and phase

constant $\beta = k_d$; here $k_d = k_0$ and can be calculated as follows

$$k_o = \frac{2\pi}{\lambda_o},\ \lambda_o = \frac{c_0}{f}$$

where $c_0 = 2.998 \times 10^8$ ms^{-1} and $f = 27$ GHz, so $\lambda_o = 1.111$ cm. Therefore,

$$k_o = \frac{2\pi}{\lambda_o} \ = 565.5 \text{ rad/m}. \tag{3.4}$$

MPM extractions: The structure is accurately modeled with the MoM. Field samples were taken for $2\lambda_0 \leq x \leq \ell$ and $z = h/10$. The number of samples $N = 300$, enough samples are taken to capture all the details for the MoM field solution.

The MPM was used to extract the propagation constants from the MoM field samples. MPM results are $\gamma_1 = 0.005 + j565.9$ (1/m) and $\gamma_2 = -0.004 - j565.9$ (1/m) with associated amplitude coefficients $C_1 = -0.0022 + j0.0012$ (A/m) and $C_2 = 0.0016 - j0.0019$ (A/m) respectively. It can be seen that β extracted by the MPM is almost the same as expected from the theory in (3.4). Even though the $\alpha \neq 0$, it is very small, so it can be neglected.

Reconstruction: The MoM fields can be reconstructed by using the MPM extracted C_m and γ_m. By putting these extracted value in (3.1) for $2\lambda_d \leq x \leq \ell$ over the length of the structure, the original near-field can be reconstructed. For the waveguide the original field was reconstructed and compared with the original MoM field, which is in the form of standing waves as shown in Fig. 3.2. It can be seen that the MPM is in excellent agreement with the MoM in reconstructing the original field.

It should be noted that the MoM sampling region starts from $x \geq 2\lambda_d$, because some unwanted evanescent wave behavior may exist near the left end due to the edge diffractions from the edges of the structure, but those will vanish after some distance, as $h < \lambda_0/2$ and only the TEM mode can be transmitted inside the waveguide.

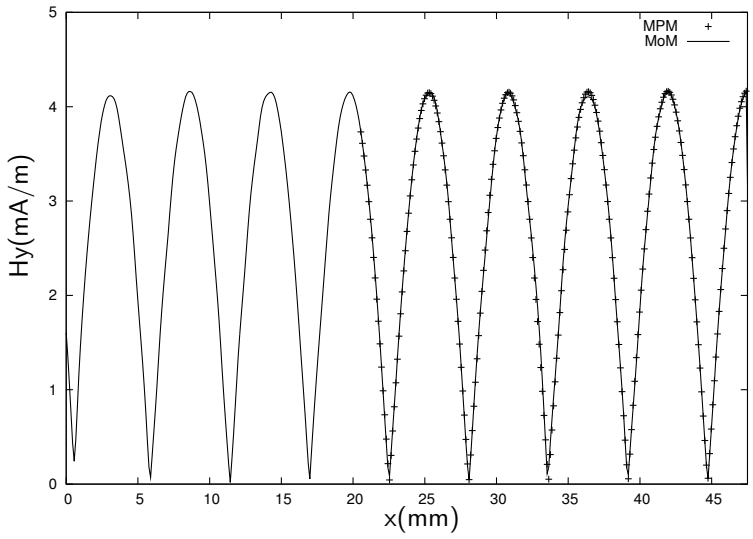

Figure 3.2: Original MoM near-field and reconstructed field using MPM extracted components.

3.2.2 Dielectric filled, short circuited parallel plate waveguide

Further verification of the accuracy of the MPM was done by increasing the complexity of the structure. The structure used in the previous section is now filled with a dielectric with $\epsilon_r = 3.5$. All the other parameters such as f, ℓ, h are kept same as before as shown in Fig. 3.3, but the wavelength λ_d and the wavenumber k_d inside the structure are not same any more. These can be calculated as

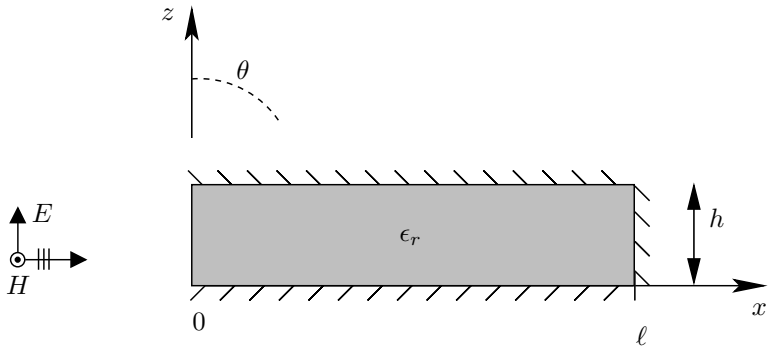

Figure 3.3: Dielectric filled parallel plate waveguide with short circuit.

$$\lambda_d = \lambda_0/\sqrt{\epsilon_r} = \frac{1.111}{\sqrt{3.5}} = 0.594 \text{ cm},$$

so,

$$k_d = k_0\sqrt{\epsilon_r} = 565.5 \times \sqrt{3.5} = 1058 \text{ rad/m}. \tag{3.5}$$

MPM Extraction: As before, the structure is modeled with the MoM and the field samples are taken inside the structure. The same sampling region criterion is used used in the previous problem, i.e., $z = h/10$ and $2\lambda_d \leq x \leq \ell$. Now, MPM extraction is done to find both the amplitude α_m as well as phase coefficients β_m for the structure. The complex propagation constants are found to be $\gamma_1 = -0.11 - j1058.9$ (1/m) and $\gamma_2 = 0.11 + j1058.9$ (1/m) with associated amplitude factors $C_1 = -0.002 - j0.0006$(A/m) and $C_2 = -0.002 - j0.0008$ (A/m) respectively. It can be seen that the β from the MPM are almost the same as those calculated above in (3.5) (i.e., $\beta \approx k_d = 1058$ rad/m). A number of verifications have been done to see that the $\alpha,\ \beta$ do not vary provided that $x \geq 2\lambda_d$.

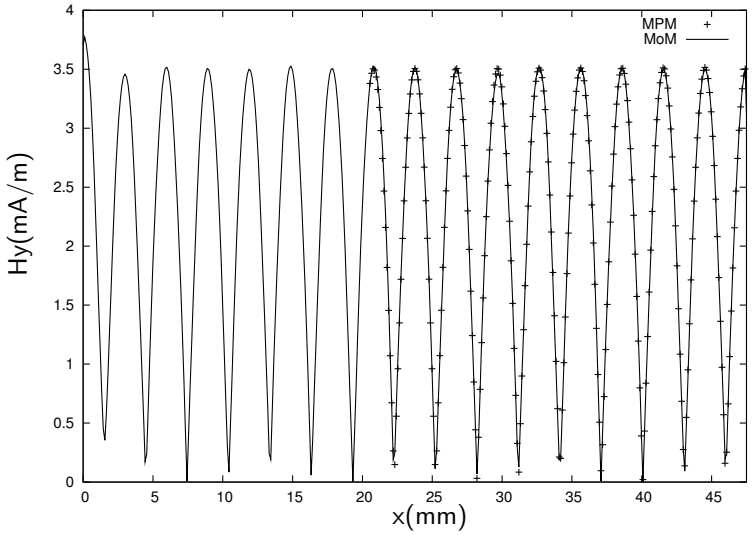

Figure 3.4: Original MoM near-field and reconstructed field using MPM extracted components.

Problem	Theory		MPM extracted	
	α (Np/m)	β (rad/m)	α (Np/m)	β (rad/m)
Air filled, short circuited	0	565.5	0.005	565.9
Dielectric filled, short circuited	0	1058	0.11	1058.9

Table 3.1: Propagation constants of air filled and dielectric filled waveguides, theoretical vs calculated.

Reconstruction: It can be seen in Fig. 3.4, even though the structure is more complex, still the original field can be recovered by using the γ_m and C_m extracted by the MPM in (3.1). So far, the MPM α_m and β_m are in excellent agreement with theoretical results of the propagation constants, and the reconstructed original fields are in excellent agreement with MoM results. The comparisons are in Table 3.1.

3.2.3 Dielectric slab waveguide on a ground plane

Another structure was analyzed using the MPM, a two dimensional "*dielectric slab waveguide with ground plane*" as shown in Fig. 3.5. The structure is modeled with the MoM ($\ell = 47.5$ mm, $h = 2.5$ mm, $\epsilon_r = 3.5$ and $f = 27$ GHz), the plane wave is incident horizontally (i.e., $\theta = -90°$). The near-field samples are obtained by using the MoM inside the structure at $z = h/10$ and $2\lambda_d \leq x \leq \ell - 2\lambda_d$ (avoiding the ends).

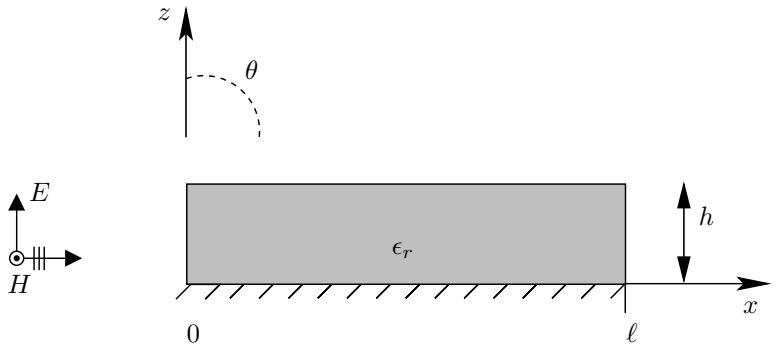

Figure 3.5: Dielectric slab waveguide on a ground plane.

MPM Extraction and Reconstruction: By using the MoM samples as the sum of complex exponentials in the MPM extractions, we obtained the propagation constants $\gamma_1 = 0.1 + j909.14$ (1/m), $\gamma_2 = 19.02 + j552.42$ (1/m), $\gamma_3 = -53.15 - j580.43$ (1/m) and $\gamma_4 = -0.36 - j908.48$ (1/m), their respective amplitude coefficients $C_1 = -0.0075 - j0.0019$ (A/m), $C_2 = 0.0024 + j0.0003$ (A/m), $C_3 = 7.12 \times 10^{-5} - j1.45 \times 10^{-6}$ (A/m) and $C_4 = 0.0013 + j0.0049$ (A/m). Here γ_1 and γ_4 represent the incident and the reflected slow wave propagation constants respectively.

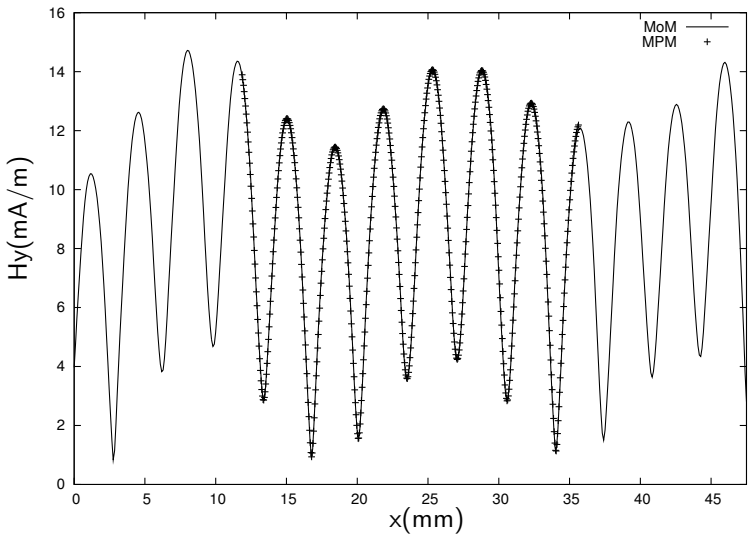

Figure 3.6: Reconstructed original field for the dielectric slab waveguide.

As in the last problem, these extracted components can be used to reconstruct the original field. By using (3.1), it can be seen in Fig. 3.6 that the MPM is in excellent agreement with the original MoM field.

3.3 Reflection coefficient

The reflection coefficient describes the amount of an electromagnetic wave that is reflected due to an impedance discontinuity in the transmission medium of that wave.

At any particular boundary, it can also be described as the ratio of the amplitude of the reflected wave to the amplitude of the incident wave at that boundary. It is denoted with Γ. It can be written as

$$\Gamma = \left.\frac{E^-}{E^+}\right|_{x=0^-} = -\left.\frac{H^-}{H^+}\right|_{x=0^-}. \tag{3.6}$$

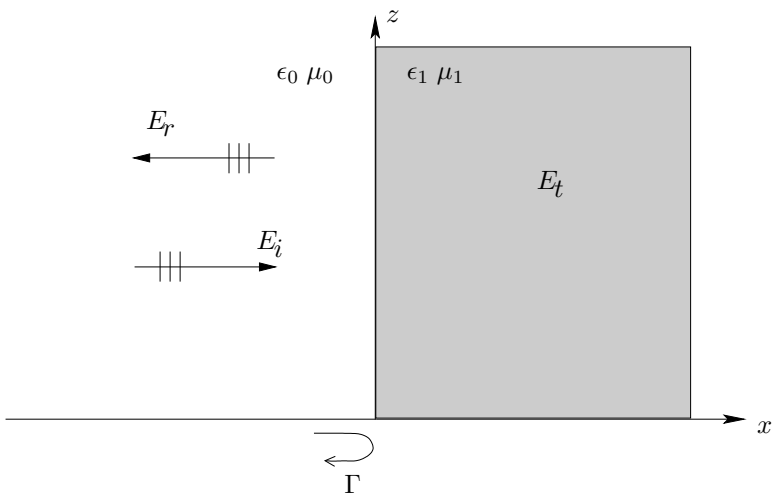

Figure 3.7: Incident wave behavior at an air-dielectric boundary.

If a plane wave with the electric field along the z-axis is incident from the free space and is propagating in $+x$ direction towards the medium as shown in Fig. 3.7, some part of the wave will get reflected as well as some part will be transmitted in the medium. In this case, the electric field reflection coefficient can be obtained by using the following expression

$$\Gamma^e = \frac{\eta_1 - \eta_0}{\eta_1 + \eta_0}, \tag{3.7}$$

where η_0 is the free space impedance and η_1 is the impedance of the dielectric, $\eta_0 = \sqrt{\mu_0/\epsilon_0}$. If we assume $\mu_1 = \mu_0$ and $\epsilon_1 = \epsilon_0\epsilon_r$

$$\Gamma^e = \frac{\sqrt{\mu_0/\epsilon_0\epsilon_r} - \sqrt{\mu_0/\epsilon_0}}{\sqrt{\mu_0/\epsilon_0\epsilon_r} + \sqrt{\mu_0/\epsilon_0}},$$

$$\Gamma^e = \frac{1-\sqrt{\epsilon_r}}{1+\sqrt{\epsilon_r}}. \tag{3.8}$$

The parameters extracted by the MPM can be used to find Γ. As we know

$$H_y(x) = C_1 e^{-\gamma_1 x} + C_2 e^{-\gamma_2 x}. \tag{3.9}$$

If we assume $\gamma_1 = \alpha + j\beta$ and $\gamma_2 = -\alpha - j\beta$, here C_1 represents the amplitude coefficient of the incident wave, and C_2 represents the amplitude coefficient of the reflected wave. So, the reflection coefficient can be calculated at any x when the values of γ_m and C_m are known. To find the magnetic field reflection coefficient at the end of the structure where $x = \ell$

$$\Gamma^h = \frac{C_2 e^{-\gamma_2 \ell}}{C_1 e^{-\gamma_1 \ell}}. \tag{3.10}$$

In the next sections, the reflection coefficient of various guiding structures will be calculated. It is expected that the MPM extracted components can be successfully used to calculate the reflection coefficient at the end of the structure that exhibits the field behavior as shown in (3.9).

3.3.1 Dielectric filled, short circuited parallel plate waveguide

A number of problems could be considered in the later sections and chapters to find the reflection coefficient of various structures. Generally, it is always good to analyze a less complex problem with some known results before moving to more complex or actual problems. For that case, a simpler two dimensional problem is analyzed as shown in Fig. 3.8. By keeping the same frequency $f = 27$ GHz, length $\ell = 47.5$ mm and height $h = 2.5$ mm with a dielectric constant inside $\epsilon_r = 3.5$, the structure is modeled in FEKO to calculate the MoM field samples inside the structure. By using

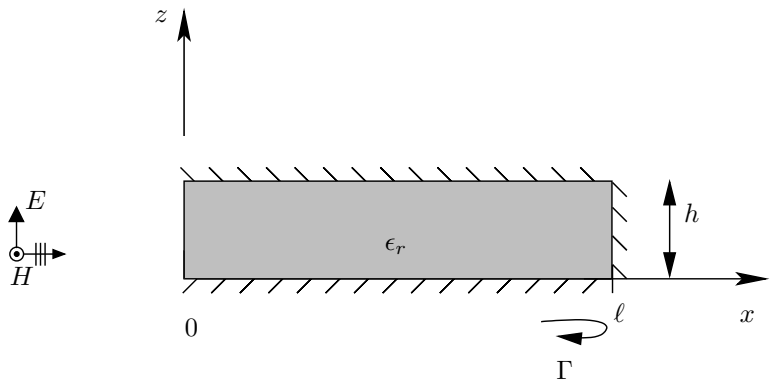

Figure 3.8: Dielectric filled, short circuited parallel plate waveguide.

the PBC it is assumed that the structure is two dimensional and there is no change in the y direction. A plane wave is incident horizontally ($\theta = -90°$), and excites the structure with E_z and H_y fields.

From a theoretical point of view for a short circuited structure like this with a perfect electric conductor (PEC) at the end, the results of Γ at the end for $\mathbf{E}$ field as well as $\mathbf{H}$ field are already known. For PEC at the load, it is known from the boundary conditions that the tangential component of the $\mathbf{E}$ field at $x = \ell$, $E_{tan} = 0$. On the other hand $H_{tan} \neq 0$. So the magnetic field reflection coefficient is

$$\Gamma^h = +1. \tag{3.11}$$

The MPM has been used for the same structure to extract C_m and γ_m in Section 3.2. For this problem $\gamma_1 = -0.11 - j1058.9$ (1/m) and $\gamma_2 = 0.11 + j1058.9$ (1/m) with associated amplitude coefficients $C_1 = -0.002 - j0.0006$ (A/m) and $C_2 = -0.002 - j0.0008$ (A/m) respectively. The incident and the reflected waves can be easily recognized from these results. Here, γ_2 and C_2 are associated with the right traveling wave because $\alpha > 0$, while the wave associated with γ_1 and C_1 is the reflected wave with $\alpha < 0$. The reflection coefficient at the load ($x = \ell$) can be calculated using

the components. Using C_m and γ_m in (3.10) at $\ell = 47.5$ mm,

$$\Gamma^h = \frac{C_2 e^{-\gamma_2 \times 0.0475}}{C_1 e^{-\gamma_1 \times 0.0475}} = 0.979\underline{/0.02^\circ}. \tag{3.12}$$

$$\boxed{\Gamma^h = 0.98}$$

It can be seen that the calculated Γ^h is in a very good agreement with the theoretical results.

3.3.2 Dielectric filled, open-ended parallel plate waveguide

The approach of calculating the reflection coefficient using MPM extractions agreed very well with theoretical results for the short circuited structure. It is expected that it would work the same way for an open ended structure shown in Fig. 3.9. For this analysis, the end of the structure has been left open.

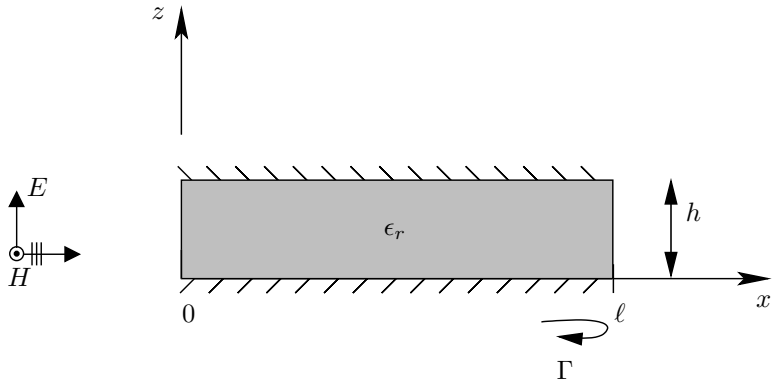

Figure 3.9: Dielectric filled, open ended parallel plate waveguide.

This problem is more complicated than we thought initially, because an incident plane wave is illuminating the structure, there are some edge diffractions going on at all the four corners of the structure. The diffractions at the end corners of the structure are causing error in the calculations of the reflection coefficient by contaminating the strength of the reflected wave. So, in order to calculate the reflection coefficient

using this approach it is required to eliminate the edge diffractions.

There are various methods to deal with the problem of the edge diffractions that arose here, but the best and the easiest way is by making the structure closed at the end. A Salisbury screen with an impedance $Z_m = 377\ \Omega$ as shown in Fig. 3.10 can be used to absorb the transmitted wave from the end.

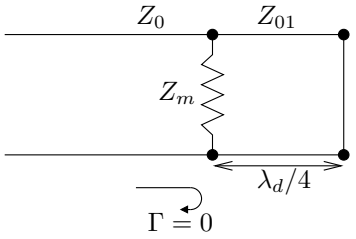

Figure 3.10: Salisbury screen.

Equivalent structure

To make the structure in a way that we can get the exact reflection coefficient at the end of the dielectric, an absorber termination with a Salisbury screen is used as shown in Fig. 3.11.

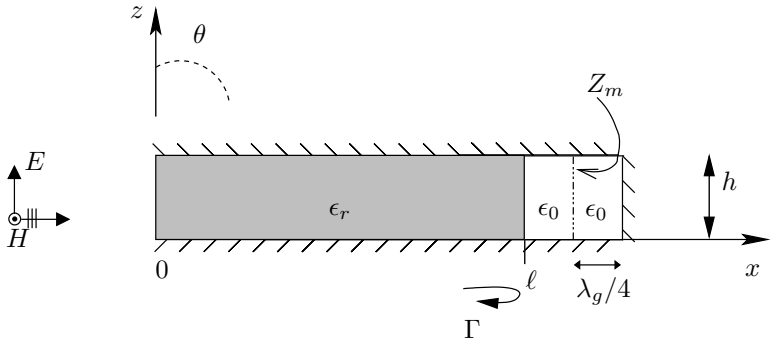

Figure 3.11: Equivalent structure to calculate reflection coefficient by using Salisbury absorbing termination to avoid the edge diffractions at the end of the structure.

In this structure, the dielectric is followed by free space, then an impedance sheet, then free space and then a short circuit (PEC). The impedance sheet is used in the

free space $\lambda_0/4$ away from the end in order to absorb the wave transmitted from the dielectric to air, and the whole structure is enclosed in a PEC except the left end (i.e., $x = 0$). Now, at $x = \ell$ we should have the exact Γ as expected for the Fig. 3.9 without any contamination due to edge diffractions. Now assuming this is a general lossless structure from (3.7)

$$\Gamma^e = \frac{\eta_0 - \eta_1}{\eta_0 + \eta_1} = \frac{\sqrt{\epsilon_r} - 1}{\sqrt{\epsilon_r} + 1}.$$

In this case $\epsilon_r = 3.5$, so

$$\Gamma^e = \frac{\sqrt{3.5} - 1}{\sqrt{3.5} + 1} = 0.3,$$

which means

$$\Gamma^h = -\,0.3. \tag{3.13}$$

The above result is the magnetic field reflection coefficient.

The equivalent structure shown in Fig. 3.11 is modeled in FEKO and near-field samples are obtained inside using the MoM. Then, the MPM is used to extract the complex amplitude and the exponential coefficients inside the structure. The complex propagation factors for the H-field are found to be $\gamma_1 = 0.22 + j1058.94$ (1/m) and $\gamma_2 = -0.62 - j1057.97$ (1/m) with $C_1 = -3.76 \times 10^{-3} + j7.91 \times 10^{-5}$ (A/m) and $C_2 = 1.06 \times 10^{-3} - j7.60 \times 10^{-5}$ (A/m). It can be seen that, γ_1 and C_1 represents the incident wave at $x = \ell$, whereas γ_2 and C_2 represents the reflected wave at $x = \ell$. So, using these components in (3.10) for $\ell = 47.5$ mm,

$$\Gamma^h = \frac{C_2 e^{-\gamma_2 \times 0.0475}}{C_1 e^{-\gamma_1 \times 0.0475}} = 0.32\ \underline{/177^\circ} \approx -0.32. \tag{3.14}$$

$$\boxed{\Gamma^h = -0.32}$$

It can be seen that the reflection coefficient calculated using the MPM extracted

Problem	Theory (Γ^h)	MPM (Γ^h_ℓ)
Dielectric filled, short circuited	$+1$	$+0.98$
Dielectric filled, open circuited	-0.3	-0.32

Table 3.2: Reflection coefficient at the load of short circuited and open ended waveguides, theoretical vs calculated.

components is in good agreement with the theoretical results.

3.4 Summary

In this chapter, various guiding structures were analyzed using the MPM, to calculate the propagation constants and reflection coefficients. A commercial EM software FEKO, which is based on the method of moments (MoM) was used to model and solve the structures for magnetic field samples inside. Then the matrix pencil method (MPM) was used to extract the propagation constants from these samples. Those components were then used to reconstruct the original field as well as to calculate the reflection coefficient. The results were validated by comparing them with the results from the EM theory of similar structures. It can been seen in Table 3.1 and Table 3.2 that the MPM is very suitable for the analysis of the guiding structures and guiding waves.

Chapter 4

2-D Leaky-Wave Antennas

4.1 Introduction

A periodic leaky-wave antenna (LWA) supports a fast space harmonic from the infinite space harmonics on the guiding structure. This fast harmonic is a fast wave that radiates or leaks the power continuously as it propagates along the guiding structure. The fast wave is also known as a *leaky wave*, for which the phase constant β is less than the free space wavenumber k_0 ($\beta < k_0$) and the attenuation constant $\alpha \neq 0$ [2]. For a LWA, α relates to represents the direction of wave travel as well as the beamwidth of the antenna, on the other hand β is associated with the direction of the beam. In FEKO, only plane wave excitation is available for 2-D structures. So, a plane wave will be used to excite the 2-D LWAs, and then the MoM field samples will be obtained. It is expected that the radiating space harmonics can be extracted using the MPM from the MoM data, and can be used to obtain the radiation pattern and reflection coefficient.

In this chapter, a two dimensional periodic LWA is being analyzed by using the matrix pencil method (MPM). In Section 4.2, the methodology behind the design of a periodic LWA is explained. The effect of the design on the radiation pattern

is explained. In Section 4.3, the MPM analysis of that periodic LWA is done by solving the structure with the MoM. In Section 4.4, the effects of edge diffraction are explained and a method to avoid those effects is presented including a novel LWA structure. In Section 4.5, the MPM extracted components are used to calculate the reflection coefficient at the end of the LWAs. In Section 4.6, the validity of this approach with infinitely long LWAs is discussed briefly. Finally, Section 4.7 is the summary of the work done in this chapter.

4.2 Leaky-wave antenna design

The matrix pencil method (MPM) has been used successfully so far for two dimensional closed top guiding structures and a dielectric slab waveguide. The performance of this method was validated by doing comparisons with other theories and results. In this section, the same approach will be used to analyze a finite length 2-D periodic leaky-wave antenna. The design of this antenna is inspired from a two dimensional LWA that was used by Encinar [24]. The metal patches are used on the top of the dielectric to make it a periodic structure.

The LWA is shown in Fig. 4.1, length $\ell = 10.2$ cm, height $h = 2.5$ mm, strip width $w = 2$ mm, period $p = 5$ mm, strip length $b = \infty$ and relative permittivity $\epsilon_r = 3.5$ is used at an operational frequency $f = 27$ GHz. This model is modeled in FEKO and periodic boundary conditions (PBC) are used make it infinite in y. The design principles related to this structure are discussed below.

4.2.1 Excitation mechanism

Plane wave excitation is used here to excite this structure at an angle of incidence $\theta_i = -90°$. It has been observed that the angle of incidence is not crucial in this finite case, because only compatible modes will be excited in the structure. So, the

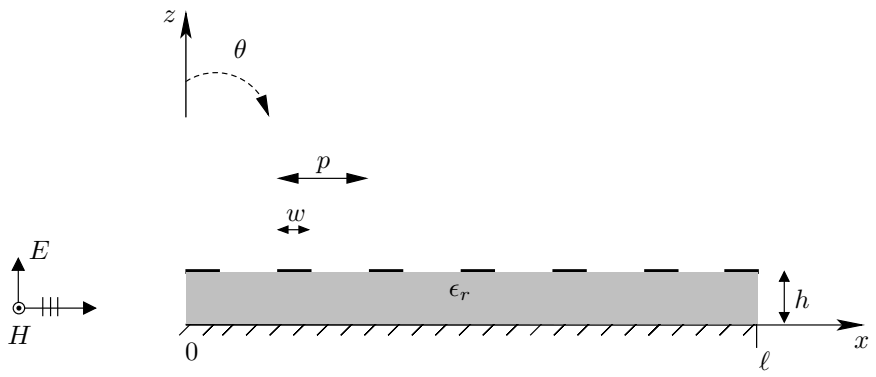

Figure 4.1: Periodic leaky-wave antenna with open dielectric end.

expected space harmonics of the LWA can be excited and hence extracted for the antenna excited from any θ_i. However, it is recommended to use $\theta_i = -90°$ in order to minimize the effect of edge diffractions at $x = \ell$. An equivalent structure to avoid the diffractions will be presented in later sections.

4.2.2 Patch dimensions and periodicity

The attenuation constant (α) of the leaky mode is responsible for the pattern beamwidth, which is dependent upon the dimensions of the patches. By keeping the period (p) constant, if we increase the strip-width (w), α decreases and so does the beamwidth.

For the purpose of avoiding the grating lobes for any scan angle, there should be a limiting value for the periodicity p. This limiting value can be determined from the Floquet harmonics [9]. The periodic structure supports a guided wave with an infinite number of Floquet space harmonics. The n^{th} harmonic has wavenumber

$$\beta_n = \beta_0 + \frac{2n\pi}{p}. \tag{4.1}$$

The Floquet $n = -1$ harmonic should be at backward endfire and the Floquet $n = 0$ mode should be at forward endfire direction. From these two conditions, the limiting periodicity to avoid grating lobes is calculated (i.e. $p/\lambda_0 = 0.5$). Hence the condition

to avoid the grating lobes is

$$\frac{p}{\lambda_0} \leq 0.5. \tag{4.2}$$

This is the very well known limitation encountered in antenna array design. In our structure, patch width $w = 2$ mm at a period of $p = 5$ mm is used as shown in Fig. 4.2, the strip length $b = \infty$.

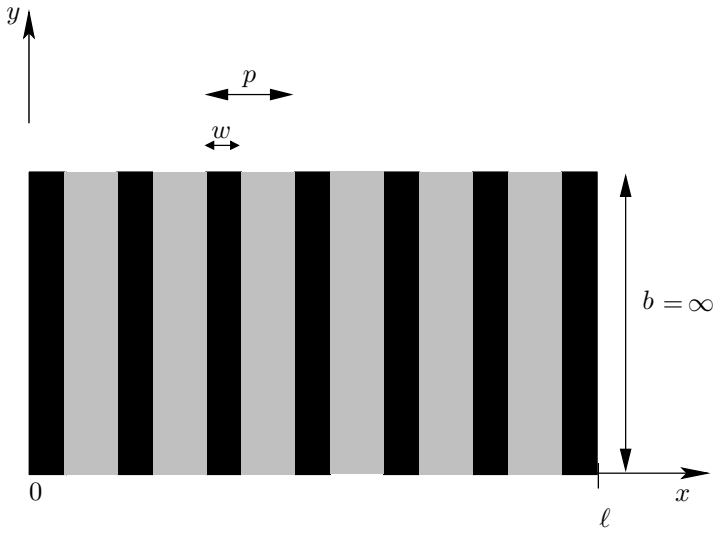

Figure 4.2: Top-view of the 2-D LWA with infinitely long metal patches.

4.2.3 Length of the antenna

The length of the antenna is responsible for the beamwidth. Also, a long antenna will reduce the reflected part of the fast wave from the end of the antenna. If the antenna is designed long enough, so that the wave traveling inside eventually vanishes when reaches at the end due to decay caused by α, the reflected wave will not exist and then the side lobe will disappear. In this study it was chosen that the amplitude of the wave should drop by -3 dB when it reaches at the end (-3 dBV$= 0.707$ V). The required length can be calculated from the following equation, choosing $\alpha \approx 3.3$ Np/m

(this choice is justified in Section 4.3)

$$e^{-\alpha\ell} = 0.707$$

$$-\alpha\ell \ln e = \ln 0.707 = -0.3454$$

$$\ell = \frac{0.3454}{3.3} \approx 10.2 \text{ cm.} \tag{4.3}$$

So, the antenna should be at least 10.2 cm long in order to get -3 dB decay in the wave traveling from $x = 0$ to ℓ. For the analysis, the antenna length $\ell = 10.2$ cm along x is used with antenna height $h = 2.5$ mm in z and the antenna width or strip length $b = \infty$ in y as shown in Fig. 4.1 and Fig. 4.2. Our objective is to just analyze the antenna characteristics using the MPM, therefore an antenna with length $\ell = 10.2$ cm is used.

4.3 Leaky wave space harmonics analysis

The same procedure as used in the previous chapter will be followed here to extract the space harmonics. This is a periodic LWA, so it is expected that there will be a fast space harmonic associated with the leaky wave. This antenna is designed in a way that just β_{-1} space harmonic will be fast and radiating harmonic.

4.3.1 MPM extractions

The structure is solved using the MoM and the field samples are taken for a region $2\lambda_d \leq x \leq \ell_0$ at $z = h/10$, where $\ell_0 = \ell - 2\lambda_d$. The idea behind this sampling region has been explained previously, i.e., there could be the effect of diffractions near the ends that can contaminate the actual results, so this sampling region avoids the ends. The field samples are then used as data for the matrix pencil extractions, which gives the components shown in Table 4.1, where $\bar{\gamma} = \gamma/k_0$, $\bar{\alpha} = \alpha/k_0$ and $\bar{\beta} = \beta/k_0$. It

Prop.	n	m	$\gamma_m = \alpha_m + j\beta_m$	C_m (A/m)
$+x$	0	1	$0.007604 + j1.685$	$-4.680 \times 10^{-3} + j8.708 \times 10^{-5}$
$+x$	-1	2	$0.007657 - j0.5367$	$5.160 \times 10^{-4} - j7.900 \times 10^{-4}$
$+x$	$-$	3	$0.007692 + j0.9996$	$1.010 \times 10^{-3} - j6.530 \times 10^{-4}$
$-x$	-1	4	$-0.007498 + j0.5369$	$-2.840 \times 10^{-4} - j9.510 \times 10^{-5}$
$-x$	0	5	$-0.007604 - j1.685$	$5.500 \times 10^{-4} - j1.400 \times 10^{-3}$
$-x$	$-$	6	$-0.09717 - j0.9862$	$9.740 \times 10^{-4} - j3.004 \times 10^{-4}$

Table 4.1: Matrix pencil extracted components of a 2-D finite periodic leaky-wave antenna.

can be seen that, there are three right-traveling and three left-traveling waves. The $m = 1$ and $m = 5$ are slow waves (with $\bar{\beta} > 1$) traveling in $+x$ and $-x$ direction respectively. The $m = 2$ and $m = 4$ components are fast waves (with $\bar{\beta} < 1$) traveling in $+x$ and $-x$ direction respectively. The $m = 3$ and $m = 6$ components seem like the space or surface waves traveling in $+x$ and $-x$ direction respectively because $\bar{\beta} \approx 1$.

This structure is designed so that the main Floquet harmonic $n = 0$ is a slow wave (corresponds to the $m = 1$ component in Table 4.1) and the $n = -1$ harmonic is a radiating fast wave (corresponds to the $m = 2$ component in Table 4.1), i.e., $-1 < \bar{\beta}_2 < +1$. As there is an infinite number of space harmonics, the MPM can be used to extract as many as we need, also (4.1) can be used to calculate the other harmonics. It has been considered that the components that follow the Floquet theory (4.1) are the only good components and those that do not follow (4.1) are not good, so the bad components are not considered in the further analysis of the 2-D LWA.

2-D strip grating: The space harmonics for a 2-D metal strip grating (which is infinite in x and y) with same strip width $w = 2$ mm, $\epsilon_r = 3.5$, $h = 2.5$ mm and frequency $f = 27$ GHz were calculated by Jackson and are shown in Table 4.2. These α and β were obtained from solving a spectral-domain periodic MoM (SDMoM) formulation (see [25] Appendix B). It should be noted that the SDMoM just gives the α and β. It does not give C_m and Γ because it is infinite in x.

p (mm)	β_0/k_0	β_{-1}/k_0	α_0/k_0
4.0	1.68145	−1.09441	0.00000
4.2	1.68357	−0.96010	0.01500
4.5	1.66930	−0.79812	0.01080
5.0	1.66389	−0.55680	0.00566
5.5	1.66116	−0.35764	0.00396
6.0	1.66038	−0.19019	0.00332
6.5	1.67416	−0.03406	0.00651
7.0	1.63281	0.04661	0.00087
7.5	1.64272	0.16227	0.00148
8.0	1.64383	0.25591	0.00167

Table 4.2: Some values α and β of an infinite 2D metal strip grating as function of period p calculated using SDMoM. Courtesy of D. R. Jackson, University of Houston.

In Table 4.2 for period $p = 5$, the $\bar{\alpha} = 0.00566$ and $\bar{\beta}_{-1} = -0.55680$. So, the MPM extracted $\bar{\gamma}_m$ in Table 4.1 are in good agreement with the theoretical $\bar{\gamma}$ computed for a 2-D strip grating using SDMoM.

4.3.2 Radiation pattern using space harmonics

The matrix pencil extracted space harmonics are in good agreement with the theoretical Floquet harmonics. Now, it is expected that these harmonics can be used to get the radiation pattern for this antenna. The radiation integral is used to construct the radiation pattern using the MPM extracted components. To use the radiation integral for this problem, the structure will be simplified using "Love's Surface Equivalent" and "Image Theory." The radiation integral is

$$H_y = e^{j\pi/4}\sqrt{\frac{k}{8\pi}}\,\frac{e^{-jk\rho}}{\sqrt{\rho}}\int_{C_0}\hat{\mathbf{y}}\cdot(\hat{\boldsymbol{\ell}}'\times\hat{\boldsymbol{\rho}})\,e^{jk\hat{\boldsymbol{\rho}}\cdot\hat{\boldsymbol{\rho}}'}\,J_\ell(\hat{\boldsymbol{\rho}}')\,d\ell'. \tag{4.4}$$

In our case, we have $H_y = H_0 e^{-\gamma x}$ (where H_0 is some constant) and $E_z = E_0 e^{-\gamma x}$, then by using Love's equivalent as shown in Fig. 4.3(a) and (b), the surface current

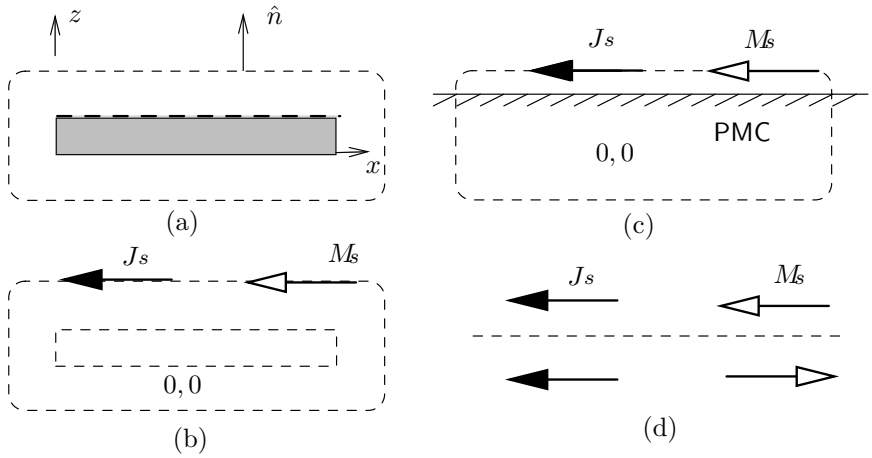

Figure 4.3: (a) Original problem with LWA. (b)Equivalent problem in free space having same fields outside the new surface. (c) Free space equivalent with a flat and infinitely long PMC inside. (d) Currents with their images due to infinite PMC surface.

$\mathbf{J}_s$ is given by

$$\mathbf{J}_s = \hat{\mathbf{z}} \times \hat{\mathbf{y}}\ H_0 e^{-\gamma x} = -\hat{\mathbf{x}} H_0 e^{-\gamma x}.$$

If we put an infinite flat perfect magnetic conductor (PMC) inside as shown in Fig. 4.3(c) and (d), it will double the electric current $\mathbf{J}_s$, on the other hand the magnetic current $\mathbf{M}_s$ will be canceled, so

$$\mathbf{J}_s = -\hat{\mathbf{x}} 2 H_0 e^{-\gamma x}.$$

From (4.4), using $k = k_o$, $\hat{\boldsymbol{\rho}} = \hat{\mathbf{x}}\ \sin\theta + \hat{\mathbf{z}}\ \cos\theta$, $\boldsymbol{\rho'} = \hat{\mathbf{x}} x'$ and $\hat{\boldsymbol{\ell}}' = \hat{\mathbf{x}}$

$$H_y = \sum_{N=0}^{n} e^{j\pi/4}\ \sqrt{\frac{k}{8\pi}}\ H_0\ \cos\theta \frac{e^{-jk\rho}}{\sqrt{\rho}}\ \int_0^{\ell} 2 e^{-(\gamma - jk_0 \sin\theta)x'} dx'. \tag{4.5}$$

So, the aperture integration of the H_y gives the far field pattern in the E plane, $\phi = 0°$,

$$H_y = H_0 \cos\theta \frac{e^{-jk\rho}}{\sqrt{\rho}}\ \frac{1 - e^{-(\gamma - jk_0 \sin\theta)\ell}}{\gamma - jk_0 \sin\theta}. \tag{4.6}$$

It can also be written as

$$H_y = f(\gamma, \theta).$$

In our case, there are two contributions to the radiation pattern, i.e, from the $+x$ traveling fast wave and $-x$ traveling fast wave. So, the total H field can be written as

$$H_y = C^+ f(+\gamma, \theta) + C^- f(-\gamma, \theta). \tag{4.7}$$

So, by using MPM extracted γ_2 and γ_4 in (4.7), the radiation pattern shown in Fig. 4.4 is obtained. Also, the SDMoM γ_m from Table 4.2 is used along with the MPM C_m in (4.7) to obtain the radiation pattern. Reciprocity is used to obtain the MoM radiation pattern.

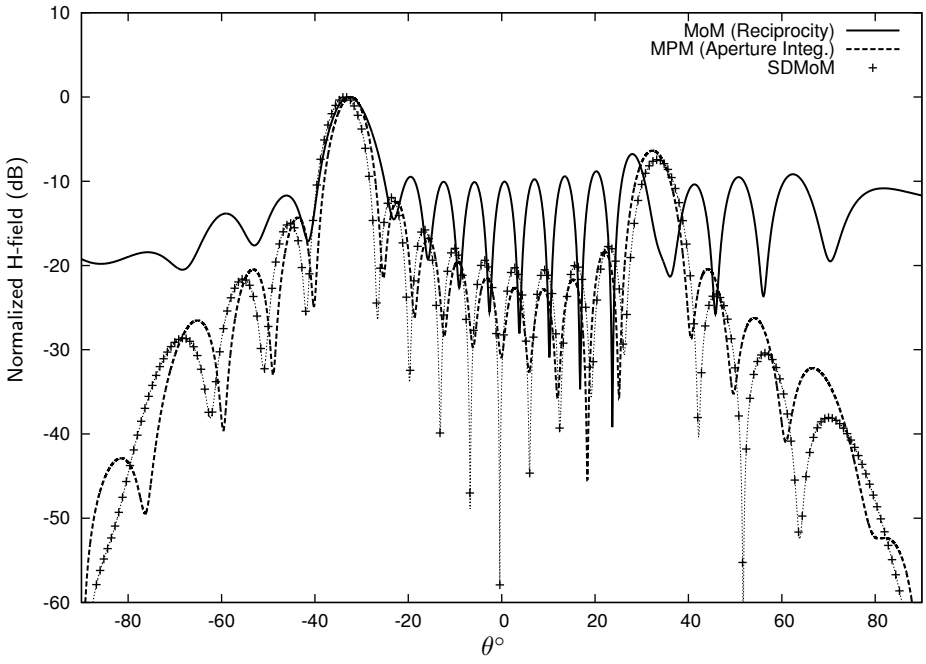

Figure 4.4: Far-field radiation pattern for the 2-D LWA obtained from reciprocity (MoM) and aperture integration, with γ from MPM and SDMoM.

It can be seen that, the radiation pattern obtained from the aperture integration of MPM extracted γ_m is in good agreement with the aperture integration of γ_m from SDMoM, as the beam angle is different by just 1° and the beamwidth is almost

same in both results. The main beam of the MPM radiation pattern is in very close agreement with the MoM and SDMoM patterns but the side lobes are not that close. It should be noted that, only the fast harmonics are considered to plot the radiation patterns.

4.4 Edge diffractions in LWA

Even though in Table 4.1, the γ_m are good, but there is a possibility of contamination of the amplitude coefficients (C_m). The reason behind this contamination is same that was addressed in the last chapter (i.e., *edge diffraction*). In Fig. 4.5(a), it can be seen that the plane wave might get diffracted at the right end of the antenna, which can cause the excitation of that end. Hence, a strong left-traveling wave could be excited

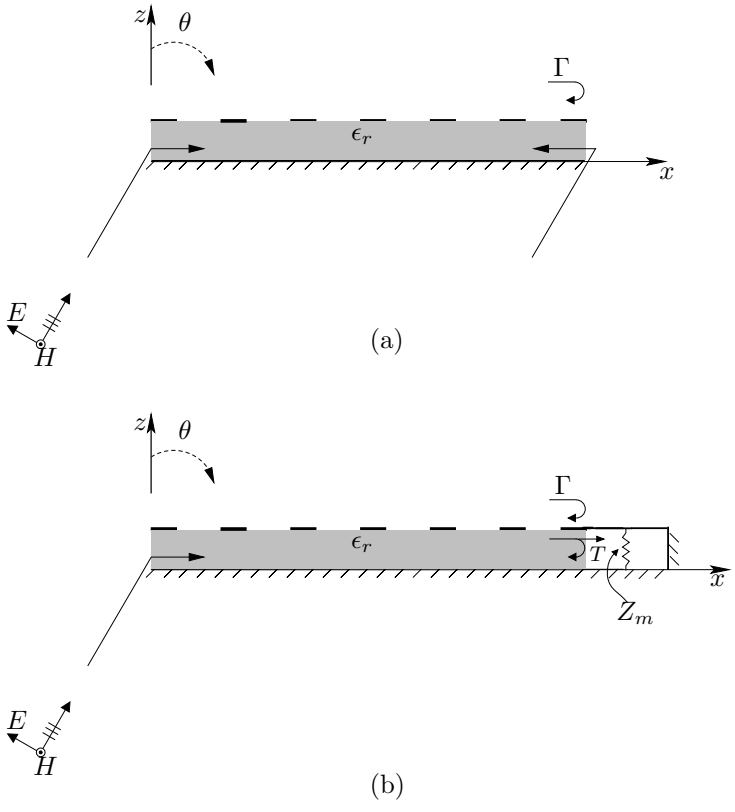

Figure 4.5: (a) Contamination of Γ in open ended LWA. (b) Closed LWA with an absorbing load to absorb the transmitted wave T.

from the right end of the antenna. In Chapter 3, a method to avoid this contamination was used by closing the end of the structure and putting a Salisbury screen at the termination. In this problem the same approach will be used, but with a different type of absorber.

4.4.1 Novel design to avoid edge diffractions

In a LWA, the contamination of the fast waves is crucial because the fast waves are radiating waves. From the right end of the antenna some part of the fast wave will be reflected back and some part will be transmitted depending on the reflection coefficient. So, if we close the structure, it is necessary to use absorb the transmitted waves (represented by T in Fig. 4.5(b)), otherwise these waves will hit the end with arbitrary angles of incidence and get reflected back. There is an artificial absorber termination available that is very effective to absorb the waves coming from a wide range of angles. It is known as "Dallenbach layer" [26]. It was used to terminate finite element mesh in [27]. The reflection coefficient of this absorber is $\Gamma = 0$.

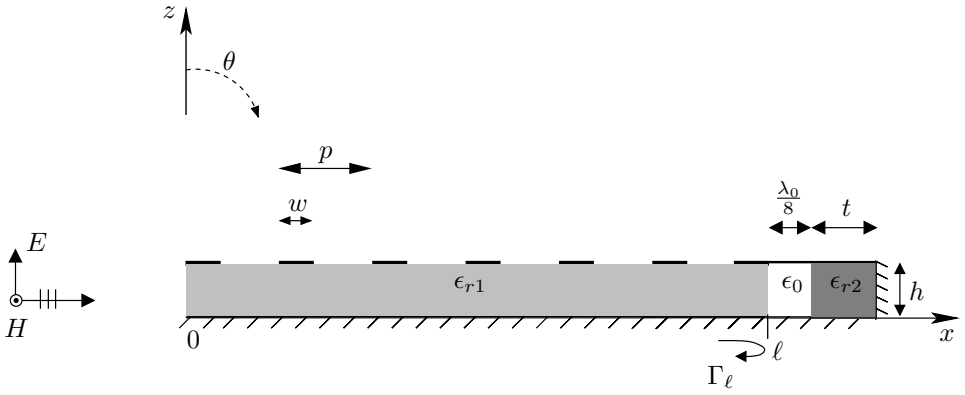

Figure 4.6: 2-D LWA with an artificial absorber termination, used to absorb the transmitted fast wave and to make C_m free from the effect of the diffractions.

The design parameters of this metal-backed absorber are kept same here, i.e., thickness $t = 0.15\lambda_0$ and relative permittivity and permeability $\epsilon_{r2} = \mu_{r2} = 1 - j2.7$. The new structure is modeled as shown in Fig. 4.6, with this extra part added at the

end of the previous antenna. There is a free space gap between two dielectrics, ϵ_{r1} and ϵ_{r2}, which could be arbitrary but here it has been chosen $\lambda_0/8$ (which is not critical). The thickness of the absorber is $t = 0.15\lambda_0$ with a PEC at the end. By using this structure, it is possible to calculate the required reflection coefficient at $x = \ell$.

The near field samples are calculated using the MoM and the space harmonics γ_m and amplitude coefficients C_m are extracted using the MPM. The fast wave γ_m and C_m are found to be

$$\bar{\gamma}_1 = \quad 0.008384 - j0.5353,\ C_1 = 6.641 \times 10^{-4} - j8.221 \times 10^{-4}\ (\text{A/m}) \tag{4.8}$$

$$\bar{\gamma}_2 = -0.007926 + j0.5358,\ C_2 = 1.652 \times 10^{-5} - j1.330 \times 10^{-4}\ (\text{A/m}). \tag{4.9}$$

The extracted γ_m and C_m can be used to obtain the radiation pattern of the antenna. By using (4.8) and (4.9) in (4.7), the radiation pattern of this new antenna is obtained and is shown in Fig. 4.7.

It can be seen that the main lobe is exactly same in both cases, on the other hand the side lobe is decreased and around -13dB. It shows that the edge diffractions from the right end were affecting the forward-pointing beam, which is associated with the reflected part of the fast wave. Hence, a more accurate reflection coefficient could be obtained from the new antenna structure with an absorber termination.

4.5 Reflection coefficient of the LWA

In Section 3.3, the MPM was successfully used to calculate the reflection coefficient at the end of the guided structures. It is expected that we can also calculate the reflection coefficient for the LWAs. Let us suppose that the $+x$ wave is in the form

$$H^+ = C^+ e^{-\gamma x}. \tag{4.10}$$

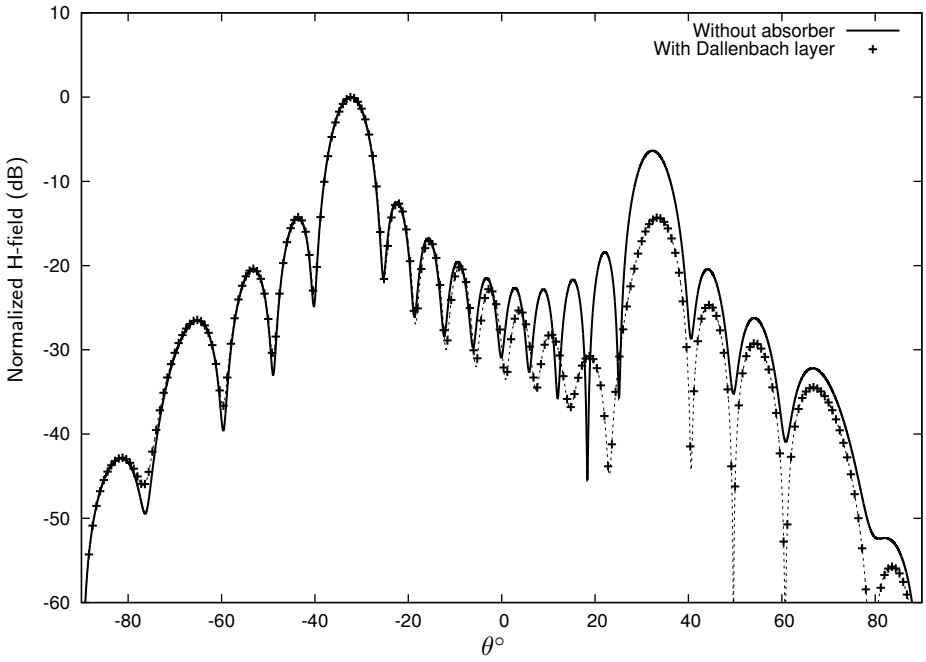

Figure 4.7: Far-field radiation patterns obtained using MPM and aperture integration for LWAs (a) with an open end and (b) with Dallenbach absorber.

Similarly, the $-x$ wave can be written as

$$H^- = C^- e^{+\gamma x}. \tag{4.11}$$

Then the reflection coefficient at the load Γ_ℓ will be

$$\Gamma_\ell = \frac{H_y^-}{H_y^+}\bigg|_{x=\ell} = \frac{C^- e^{+\gamma\ell}}{C^+ e^{-\gamma\ell}}. \tag{4.12}$$

Two LWAs has been analyzed using the MPM in this chapter. The above equation can be used to calculate the reflection coefficient from MPM extracted components of those antennas.

2-D LWA open ended

By using γ_m and C_m for the fast waves from Table 4.1 in (4.12),

$$\Gamma_\ell = \frac{C_4 e^{-\gamma_4 \ell}}{C_2 e^{-\gamma_2 \ell}}$$

where C_2 and C_4 represent C^+ and C^- respectively. So,

$$\Gamma_\ell = 0.76\underline{/-53^\circ}. \tag{4.13}$$

$$\boxed{|\Gamma_\ell| = 0.76}$$

2-D LWA with an absorber termination

By using (4.11) and (4.12) in (4.15)

$$\Gamma_\ell = \frac{C_2 e^{-\gamma_2 \ell}}{C_1 e^{-\gamma_1 \ell}},$$

$$\Gamma_\ell = 0.33\ \underline{/28^\circ}. \tag{4.14}$$

$$\boxed{|\Gamma_\ell| = 0.33}$$

It can be seen that the reflection coefficient has changed after using the absorber termination. There might be many factors that can affect the reflection coefficient in these cases. It was expected that by closing the right end of the antenna the edge diffractions can be avoided, and it has been proved here that the edge diffractions were affecting the field, which are eliminated by using the Dallenbach layer.

4.6 Infinite leaky-wave antenna analysis

The finite two dimensional antenna used in the previous analysis is now changed to an infinite structure, which is infinite in both x and y directions as shown in Fig. 4.8. The same idea of putting PBCs is used here to make it infinite while keeping the

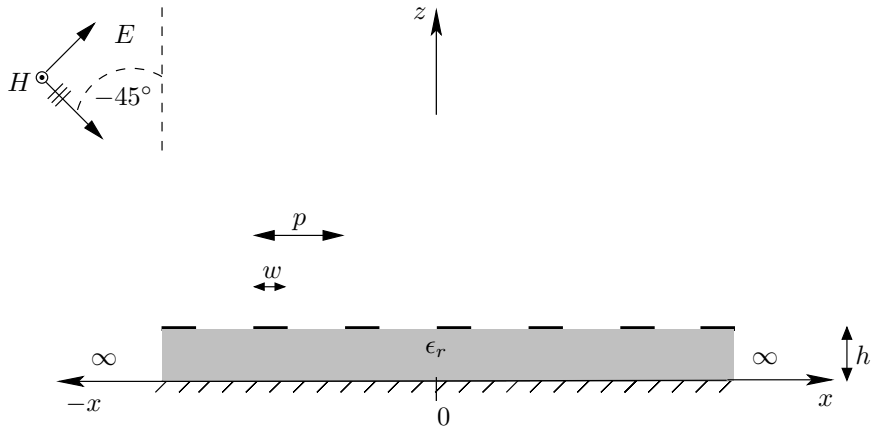

Figure 4.8: 2-D infinite periodic LWA with plane wave incident from $\theta = -45°$.

same period $p = 5$ mm, height $h = 2.5$ mm and strip width $w = 2$ mm at a frequency of $f = 27$ GHz. The plane wave excitation is chosen at an angle $\theta_i = -45°$, though any arbitrary angle can be chosen as it is not critical.

4.6.1 Space harmonic extractions

The antenna structure was solved with the MoM solver and field samples were taken inside the structure at $z = h/10$. These MoM samples were used in the matrix pencil method (MPM) to extract the space harmonics. It is found that the extracted space harmonics are dependent on the angle of incident plane wave. The value of β changes with changing the θ_i. So, this analysis can not be done with MPM for an infinitely long two dimensional LWA because it is not possible to find β using this approach.

4.7 Summary

In this chapter, a two dimensional leaky wave antenna with periodic metal strips on the top was analyzed. The antenna structure was modeled in FEKO and MoM based solutions were taken and used for the MPM extractions. The propagation constants and the attenuation constants were extracted and then compared with the Floquet space harmonics for the same period. The Floquet harmonics provided β_n that agree with the MPM results. The extracted attenuation constants α_m were also verified by comparing with the SDMoM α for 2-D strip grating.

The extracted harmonics were then used in the radiation integral to plot the radiation pattern, which was then compared with the radiation pattern from the known α and β. The calculated pattern was in agreement with only 1° beam-direction difference from the theory results of the metal strip grating.

The effects of edge diffractions were introduced, and a termination with a Dallenbach layer was used to eliminate those effects. The LWA structure was then analyzed using the MPM to obtain the radiation pattern. The method to calculate the reflection coefficient from the MPM extracted components was explained. By using that method, it was found that the reflection coefficient of 2-D LWA was improved. An infinite antenna was also analyzed with the same approach but it was found that this approach was not suitable for an infinite antenna.

Chapter 5

3-D Leaky-Wave Antennas

5.1 Introduction

For the 2-D leaky-wave antennas, it was seen that the leaky waves are fast waves with wavenumber $-k_o \leq \beta \leq k_0$ and can be extracted using the MPM. From a practical point of view, analysis of 3-D LWAs is more desirable. It is expected that the same approach could be used in 3-D LWAs. The main focus of this chapter is on the calculation of a reflection coefficient and radiation pattern from the MPM extracted components. In FEKO, we have magnetic dipoles for the excitation of 3-D structures. So, the structure is excited using an array of magnetic dipoles to approximate a uniform line source. Also, the MoM radiation pattern is available directly for 3-D LWA. So, it would be interesting to obtain the radiation pattern from the aperture integration of the extracted components and compare with the MoM radiation pattern.

This chapter starts with modifications of the previously used leaky-wave antenna to make it a 3-D LWA. In Section 5.3, the MPM analysis of the 3-D antenna is done to extract the space harmonics. In Section 5.3.3, the radiation integral is used to get the radiation pattern which then compared with the FEKO pattern. The existence and

the effects of other space harmonics are also described in Section 5.3.4. The MPM extracted components are then used to calculate the reflection coefficients for the LWA in Section 5.4. The required comparisons with the SDMoM results have been done in Section 5.3. In Section 5.5, the behaviors of 2-D and 3-D LWAs are compared, the effects of strip length on the antenna behavior are explained and analyzed. Finally, the chapter is summarized in Section 5.6.

5.2 Antenna design

The characteristics of a 3-D periodic unidirectional LWA shown in Fig. 5.1 will be analyzed using the MoM and MPM. The design of the antenna is similar to the one

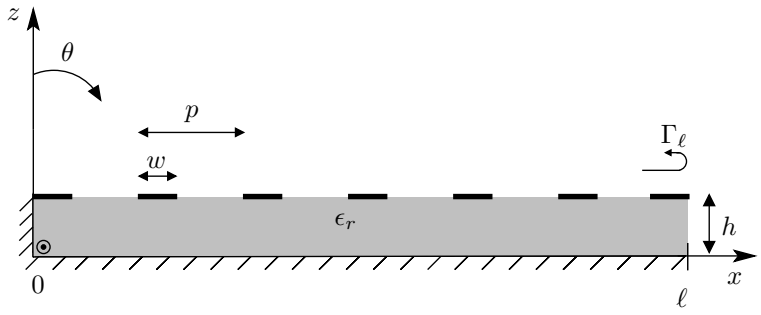

Figure 5.1: 3-D finite periodic unidirectional LWA with metal patches on the top.

used in the last chapter, except this is now a three dimensional structure, which means it is finite in y. The strip length $b = 5$ mm is used here in y as shown in Fig. 5.2. The other parameters are kept same (i.e., $\ell = 10.2$ cm, $h = 2.5$ mm, $p = 5$ mm, $w = 2$ mm, $\epsilon_r = 3.5$ and $f = 27$ GHz).

The excitation mechanism is different in this antenna from the 2-D LWAs. We are assuming the TM_x polarization ($\bar{H} = \hat{\mathbf{y}} H_y$) so an array of three magnetic dipoles is used near the origin inside the structure to approximate a uniform line source of finite length b. The strength of each dipole is $b/3 = 1.67 \times 10^{-3}$ V-m [28], which is equivalent to a uniform line source of length b. The left end is replaced by a PEC to

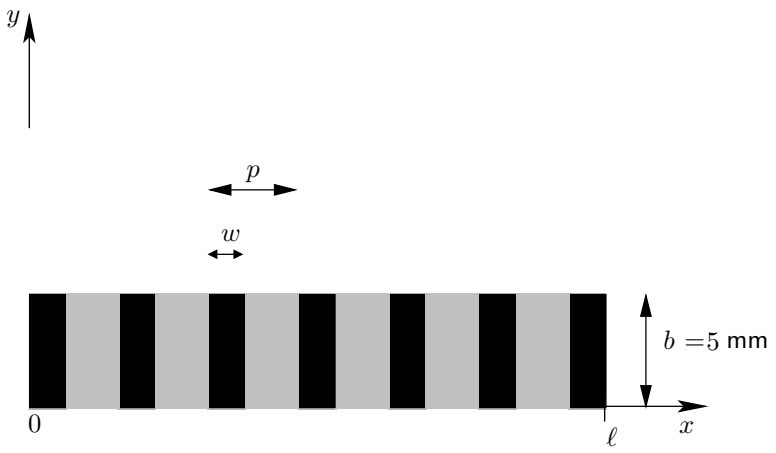

Figure 5.2: Top view of the 3-D periodic LWA.

make it a unidirectional LWA. The right end of the antenna is kept open.

5.3 Leaky-wave analysis

The propagation constant γ plays a major role in determining the overall antenna characteristics. As discussed previously, the antenna beamwidth depends upon the attenuation constant α, on the other hand the beam angle is dependent upon the phase constant β. The fundamental harmonic of a LWA is a slow (non-radiating) wave along the length of the structure, with a phase constant $\beta > k_0$. In the periodic structure the slow wave radiates from the discontinuities at the end of the structure [2]. The periodic discontinuities create a guided wave with an infinite number of space harmonics (Floquet space harmonics). The nth Floquet wave has a wavenumber as follows,

$$\beta_n = \beta_0 + \frac{2n\pi}{p} \tag{5.1}$$

where p is the period. This structure is designed so that the main harmonic $n = 0$ is a slow wave and $n = -1$ harmonic is a radiating fast wave (i.e., $-k_0 < \beta_{-1} < k_0$). These space harmonics can be extracted for 3-D LWAs by using the same approach that was used in previous chapter.

5.3.1 MPM extraction of space harmonics

The structure was modeled and the MoM solution for the magnetic field H_y was calculated just above the aperture. For the MoM, samples are taken along x above the top of the antenna at $z = h + 0.01$ mm for $2\lambda_d \leq x \leq \ell_0$, where $\ell_0 = \ell - 2\lambda_d$. Then these samples were used as an input to the MPM. By using the MPM, the most dominant space harmonics were extracted and are shown in Table 5.1, where $\bar{\gamma} = \gamma/k_0$, $\bar{\alpha} = \alpha/k_0$ and $\bar{\beta} = \beta/k_0$. 500 field samples were used here, because otherwise we can not get a good α.

n	Prop.	m	$\bar{\gamma}_m = \bar{\alpha}_m + j\bar{\beta}_m$	C_m (A/m)
0	$+x$	1	$0.02047 + j1.539$	$-0.3074 + j0.04773$
-1	$+x$	2	$0.01956 - j0.6807$	$-0.2313 - j0.1667$
-1	$-x$	3	$-0.02448 + j0.6832$	$0.01375 + j0.006406$
0	$-x$	4	$-0.01947 - j1.536$	$-0.01953 - j0.005820$
$-$	$+x$	5	$0.07821 + j0.9843$	$0.02475 + j0.05080$
-2	$+x$	6	$0.02044 - j2.902$	$-0.04550 - j0.01169$
$+1$	$+x$	7	$0.01731 + j3.765$	$0.008167 + j0.02898$
$-$	$-x$	8	$-0.1147 - j0.9572$	$0.01322 + j0.006017$

Table 5.1: Matrix pencil extracted propagation constants and amplitude coefficients of 3D periodic leaky-wave antenna.

It can be seen in Table 5.1, the $m = 1$ and $m = 2$ components are the most dominant waves with the largest amplitude coefficients C_1 and C_2 respectively. The direction of the waves can be recognized very easily from the sign of α. The components with $\bar{\alpha} > 0$ are associated with the waves traveling in the $+x$ direction, on the other hand the components with the $\bar{\alpha} < 0$ are associated with the waves traveling in the $-x$ direction.

This structure is designed so that the main harmonic $n = 0$ is a slow wave (corresponds to the $m = 1$ component in Table 5.1) and the $n = -1$ harmonic is a radiating fast wave (corresponds to the $m = 2$ component in Table 5.1), i.e., $-1 < \bar{\beta}_2 < +1$. It also has been observed that the other components extracted using the MPM closely

follow the behavior prescribed by (5.1). These MPM γ_m for 3-D LWA are not that close to the MPM γ_m of 2-D LWA (Table 4.1) and SDMoM γ_m (Table 4.2).

5.3.2 Components behavior verifications

The behavior of the space harmonics can be analyzed further to see the behavior of slow harmonics. It is expected that the slow harmonic is evanescent in z. It decays exponentially in the $+z$ direction. So, the MoM samples were taken at several different values of z (i.e., $z = h + d$), where d is the distance of the sampling region from the top of the antenna and the γ_m and C_m were extracted for each d.

d (mm)	$\bar{\gamma}_m = \bar{\alpha}_m + j\bar{\beta}_n$	C_m (A/m)
0.01	$0.002047 + j1.539$ $0.01956 - j0.6807$	$-0.3074 + j0.04773$ $-0.2313 - j0.1667$
1	$0.02056 + j1.541$ $0.01966 - j0.6813$	$-0.1404 + j0.01338$ $-0.2263 - j0.09303$
5	$0.02056 + j1.541$ $0.01980 - j0.6813$	$-0.007617 - j0.001517$ $-0.07633 + j0.1188$

Table 5.2: Matrix pencil extracted propagation constants and associated amplitude coefficients at different heights from the top of the LWA.

In Table 5.2, it can be seen that as we go further away from the antenna, the slow wave harmonic is getting weaker and weaker. At a distance of $d = 0.01$ mm, the slow wave was stronger than the fast wave. As we increased the distance to $d = 1$ mm, the strength of the fast wave was dropped to less than 50% of the strength at $d = 0.01$ mm. As the distance was increased further to $d = 5$ mm, the strength of the slow wave was further dropped by almost 18 times, on the other hand the fast wave strength is still around 50% of what it was at $d = 0.01$ mm. It has been observed that if we increase the distance even more, eventually the slow wave disappears. So, the matrix pencil components are behaving exactly as it was expected from the theory of the leaky waves and guided waves.

5.3.3 Radiation pattern of the LWA

The radiation pattern of the 3-D LWA can be calculated easily using the MoM. It is expected that to plot the radiation pattern, the MPM extracted components can be used in the radiation integral. In the previous chapter the same approach was used to obtain the radiation pattern of the 2-D LWA. This antenna is a 3-D version of the antenna used in the previous chapter, so the aperture integration of H_y from (4.7) gives the far field pattern in E plane, $\phi = 0°$,

$$H_y = H_0 \cos\theta \frac{e^{-jkr}}{r} \frac{1 - e^{-(\gamma - jk_0 \sin\theta)\ell}}{\gamma - jk_0 \sin\theta}, \tag{5.2}$$

where H_0 is some constant. It can also be written as

$$H_y = f(\gamma, \theta).$$

In our case, there are two contributions to the radiation pattern, i.e, from the $+x$ traveling fast wave and $-x$ traveling fast wave. So, the total H field can be written as

$$H_y = C^+ f(+\gamma, \theta) + C^- f(-\gamma, \theta). \tag{5.3}$$

The radiation pattern is obtained for $-90° \leq \theta \leq +90°$ by using MPM extracted fast wave components from Table 5.1 in (5.3), and shown in Fig. 5.3. It is also compared with the MoM results. Both the MoM pattern and MPM reconstruction are in good agreement with one another.

It can be seen that a good agreement has been made with the MoM results in terms of the main beams, but the side lobes are little bit different from the MoM result. There are number of possible reasons that could affect the side lobes in this problem. The MoM result is for a three dimensional problem, whereas the radiation integral is solved by assuming that the aperture is just two dimensional. Also, there

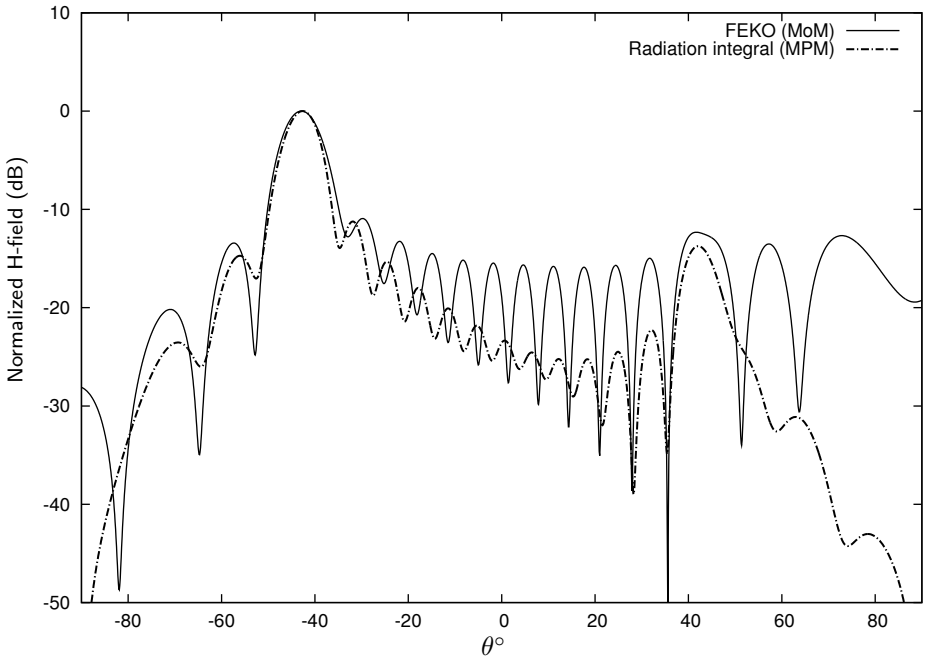

Figure 5.3: Far-field pattern comparison of the MPM and the MoM.

could be some contribution due to the space wave that is coming directly from the source, it can affect the radiation pattern.

5.3.4 Other components

From Fig. 5.3, it can be seen that there is possibility of the presence of more than two components in the radiation pattern. It is possible that there is a wave which is coming directly from the source and affecting the radiation pattern as shown in Fig. 5.4. In the MPM extracted $\bar{\gamma}_5 = 0.07821 + j0.9843$ and $\bar{\gamma}_8 = -0.1147 - j0.9572$ look like space waves, as $\bar{\beta} \approx 1$, but the space waves can not be defined as the sum of the complex exponentials, so these other MPM extracted components are not purely space waves.

Using $m = 2,\ 3,\ 5$ and 8 components from Table 5.1, the radiation pattern is obtained using (5.3) and plotted in Fig. 5.5. It can be seen that the side lobe around $\theta = 42^\circ$ is little bit improved, it is expected that the side lobes can be tuned by tuning

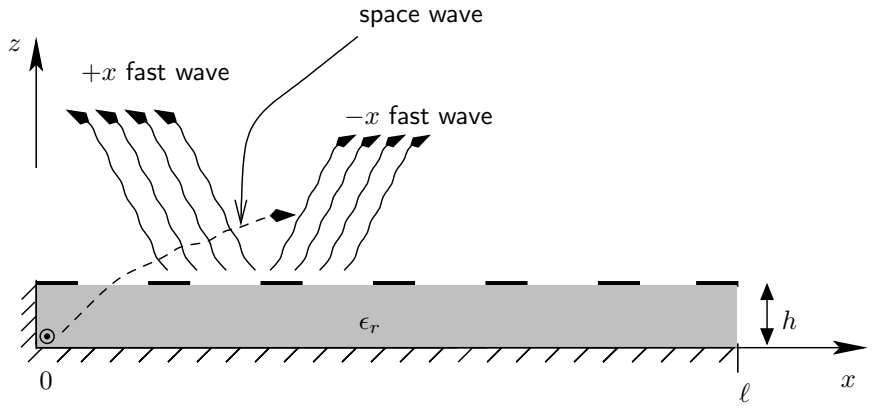

Figure 5.4: Behavior of forward and backward fast-waves and effect of space-wave coming directly from the source.

the space waves. But the radiation pattern obtained from the aperture integration of the fast wave components is in good agreement with the MoM radiation pattern. In the radiation pattern of the antenna, there might be a space wave term e^{-jkr}/r, and the MPM extractions are not suitable for the reconstruction of this term. It

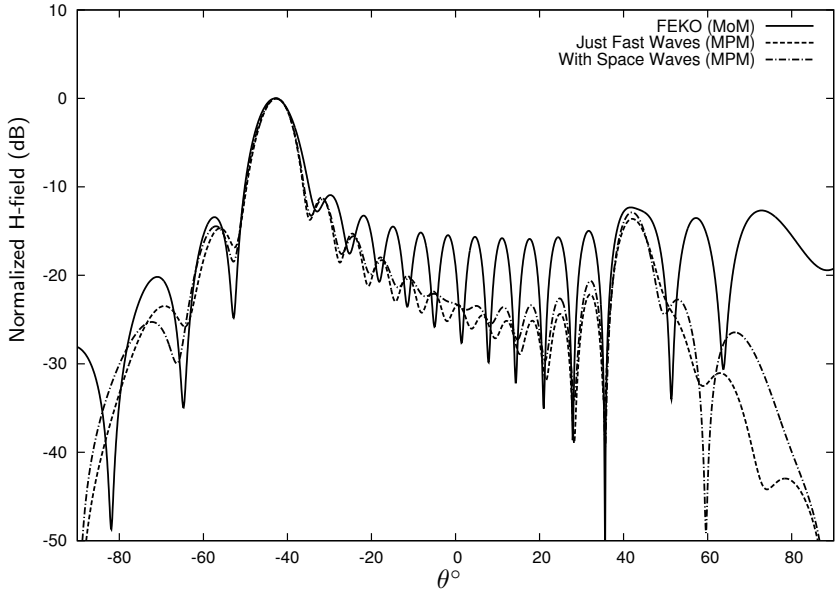

Figure 5.5: Radiation patterns of 3-D LWA: from FEKO and aperture integration (using just fast waves and fast waves plus other components).

seems like the MPM tried to extract this term but failed and gave us the components

those are not following the Floquet theory. Therefore, these components were ignored during the analysis of LWAs in this thesis.

5.4 Reflection coefficient of the LWA

In Section 4.5, the MPM was used to calculate the reflection coefficient at the end of the 2-D LWA. In the 3-D LWA, the mechanism of radiation is the same, so, $+x$ traveling and $-x$ traveling waves can be written as

$$H^+ = C^+ e^{-\gamma x}, \tag{5.4}$$

$$H^- = C^- e^{+\gamma x}. \tag{5.5}$$

So, the reflection coefficient Γ_ℓ at the load is

$$\Gamma_\ell = \left.\frac{H_y^-}{H_y^+}\right|_{x=\ell} = \frac{C^- e^{+\gamma \ell}}{C^+ e^{-\gamma \ell}}. \tag{5.6}$$

In our case, it is expected that two methods can be used to calculate the Γ, as follows:

A. Using MPM extracted components

In order to calculate the reflection coefficient at the load, the MPM extracted components can be used from Table 5.1 in (5.6),

$$\Gamma_\ell = \frac{C_3 e^{-\gamma_3 \ell}}{C_2 e^{-\gamma_2 \ell}} = 0.67\underline{/-22^\circ}. \tag{5.7}$$

$$\boxed{|\Gamma_\ell| = 0.67}$$

B. Using the radiation pattern

The far-field pattern shown in Fig. 5.3 can be used to find an approximate reflection coefficient at the load. In this LWA, the main beam is associated with

the $+x$ traveling fast wave, on the other hand the forward beam is associated with the $-x$ traveling fast wave. So, the strength of the main beam will be maximum when the strength of the $+x$ fast wave is maximum, likewise the side beam strength is maximum when the $-x$ fast wave strength is maximum. From the pattern shown on Fig. 5.3, we can see that the forward beam is around -12 dB weaker than the main beam (i.e., -12 dB $= 0.25$).

The radiation pattern's forward beam can be related to the reflection coefficient in terms of the ratio of the forward beam to the main beam. In other words the reflection coefficient can be used to predict the ratio of forward to backward pointing beams,

$$\frac{|H_y(\theta = +43^\circ)|}{|H_y(\theta = -43^\circ)|} = |\Gamma_\ell| e^{-\alpha_2 \ell} = 0.22.$$

This ratio ($0.22 \approx -13$ dB) is in good agreement with the pattern in Fig. 5.3. So by using this idea, the reflection coefficient can be calculated from the pattern if we know the fast wave propagation constants as follows,

$$\Gamma_\ell = \frac{|H_y(\theta = +43^\circ)|}{|H_y(\theta = -43^\circ)|} e^{+\alpha_2 \ell}. \tag{5.8}$$

5.5 2-D and 3-D LWAs pattern comparisons

The 2-D and 3-D models of LWAs have been analyzed, and it has been observed that even the design parameters of both antennas are same but the radiation pattern of 3-D LWA is different from that of 2-D antenna. The beam angle of 2-D LWA used in previous chapter was $\theta_b^{2D} \approx -32.4^\circ$, and the beam angle of the infinite 2-D metal strip grating using the SDMoM β_{-1} from Table 4.2 is $\theta_b^{SDMoM} \approx -34^\circ$, but the beam angle of 3-D LWA with strip length $b = 5$ mm is $\theta_b^{3D} \approx -43^\circ$. Even though 2-D and 3-D models produce different radiation patterns, it is possible make them in a reasonable agreement with one another.

5.5.1 Effect of strip length on radiation pattern

Various 3-D LWAs with different strip lengths were tested for this analysis. An antenna with the strip length $b = 20$ mm is used keeping $p = 5$ mm, $w = 2$ mm, $h = 2.5$ mm and $f = 27$ GHz is analyzed as shown in Fig. 5.6. The excitation mechanism is same but 12 magnetic dipoles array is used here to approximate a uniform source To analyze this antenna with longer strips, the MoM near field samples were taken

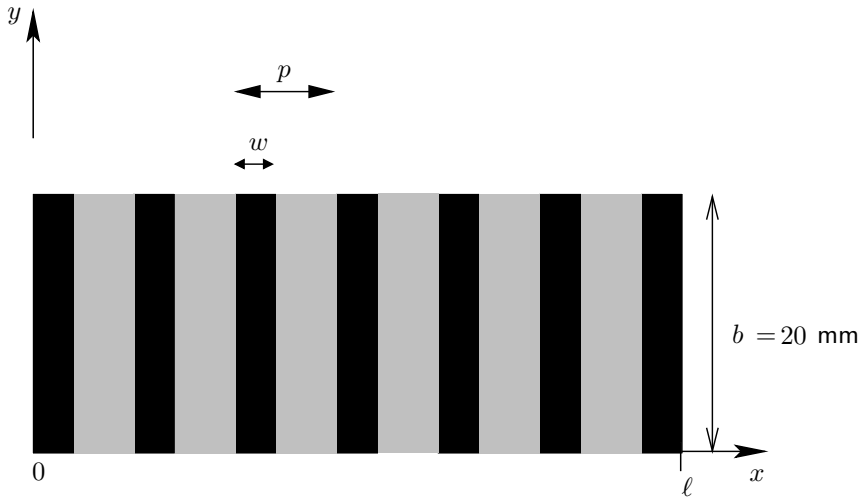

Figure 5.6: Top view of new LWA with increased strip length.

and used in the MPM extractions. The MPM extracted fast wave components of the new 3-D LWA are

$$\bar{\gamma}_1 = 0.008987 - j0.5625,\ C_1 = -0.2943 - j0.1073 \text{ A/m} \tag{5.9}$$

$$\bar{\gamma}_2 = -0.0009252 + j0.5671,\ C_2 = 0.07048 - j0.04580 \text{ A/m}. \tag{5.10}$$

The radiation pattern was obtained from the MoM. The radiation pattern of the 2-D LWA with $b = \infty$ (aperture integration of the MPM components), and 3-D LWAs with $b = 5$ mm and $b = 20$ mm are compared in Fig. 5.7. It can be seen that by changing the strip length, the angle of the main beam and side beam changes. The

main beam angle changes from $\theta_b \approx -43^\circ$ to $\theta_b \approx -34^\circ$, which is just 2° away from the main beam of 2-D LWA pattern obtained using the MPM extracted components in the previous chapter.

It should be noted that by changing the strip length, the forward beam becomes stronger, as shown in Fig. 5.7, which means there could be a change in the attenuation constant α or the reflection coefficient Γ of the antenna. It can be seen that α and

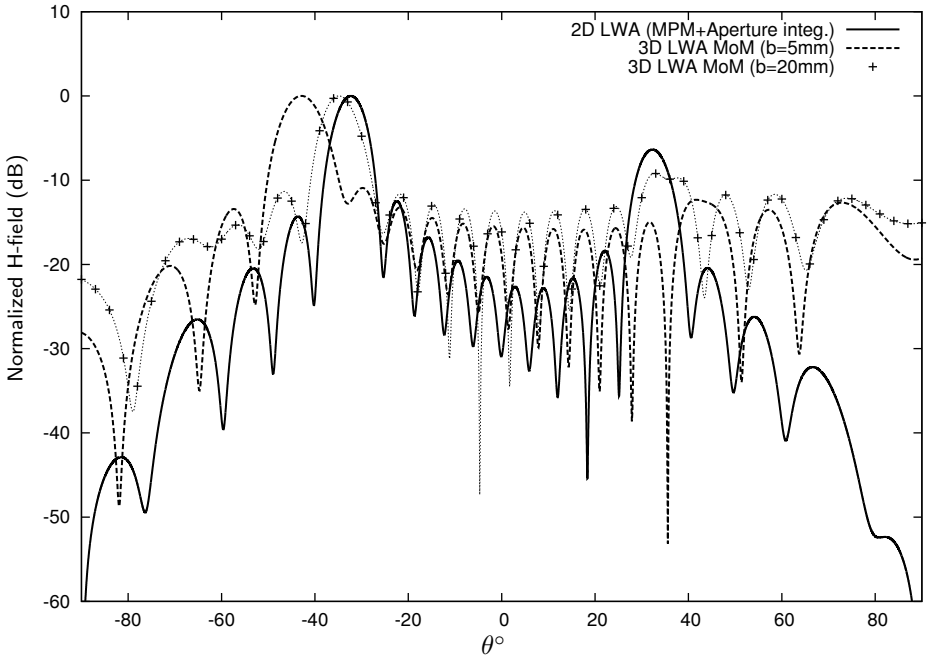

Figure 5.7: Radiation patterns of 3-D LWAs from FEKO and 2-D LWA from MPM extracted components.

β are changed by increasing the strip length. The MPM components are close to the SDMoM components from Table 4.2, i.e., $\bar{\gamma} = 0.00566 - j0.5568$. So, the antenna with the longer strips is in a good agreement with 2-D MPM results as well as SDMoM results for an 2-D strip grating.

5.5.2 Reflection coefficient

The propagation constants are changed by changing the strip length, which means it will also affect the reflection coefficient of the antenna. So, by using (5.9) and (5.10) in (5.6)

$$\Gamma_\ell = \frac{C_2 e^{-\gamma_2 \ell}}{C_1 e^{-\gamma_1 \ell}}$$

$$\Gamma_\ell = 0.47 \angle -6^\circ. \tag{5.11}$$

$$\boxed{|\Gamma_\ell| = 0.47}$$

Using (5.8)

$$\frac{|H_y(\theta = +34.5^\circ)|}{|H_y(\theta = -34.2^\circ)|} = |\Gamma_\ell| e^{-\alpha_1 \ell} = 0.28.$$

This ratio ($0.28 = -11$ dB) is in a good agreement with Fig. 5.7.

5.6 Summary

In this chapter, a three-dimensional leaky wave antenna with periodic metal patches on the top was analyzed. The antenna structure was modeled in FEKO and solved with the MoM. The MoM field samples were used in the MPM extractions. The propagation constants and the attenuation constants were extracted and then compared with the Floquet space harmonics. The evanescent mode behavior was expected from the theory of LWAs, so the field samples were taken at different heights from the top of the antenna and the MPM was used to extract the complex components at those heights. It has been verified that the fast-wave component is getting more and more dominant as we increase the height of the sampling region above the aperture, because the slow harmonic is getting weaker and weaker.

The radiation pattern of the antenna was obtained using the MPM components in the aperture integration. The effects of two other components in the radiation pattern were also considered. It was found that some components with $\bar{\beta} \approx 0$ were

slightly affecting the side lobes in the radiation pattern, but the pattern from the aperture integration of just fast wave components was in good agreement with the MoM radiation pattern.

The reflection coefficient of the LWA was also calculated. The reflection coefficient calculated from the MPM extracted fast harmonics was in excellent agreement with the reflection coefficient calculated from the MoM radiation pattern.

The effects of the strip length were also analyzed. It was observed that by increasing the strip length of the 3-D LWA, the antenna radiation behavior became very close to the 2-D LWA. It was also found that the MPM extracted fast $\bar{\gamma}_m$ are in good agreement with the SDMoM results of the 2-D strip grating. The reflection coefficient of the new design with longer strips was also calculated using the MPM extracted components.

Chapter 6

Conclusions

In this thesis, the utilization of the matrix pencil method to analyze the closed top guiding structures and leaky-wave antennas has been investigated. The MPM can be be used to extract the complex propagation constants γ_m from the MoM field samples. Once the γ_m are calculated, the least-squares method can be used to extract the amplitude coefficient C_m. Then the radiation pattern of the LWAs can be obtained by using the γ_m and C_m associated with the radiating or leaky mode in the aperture integration. The reflection coefficient for any specific mode can be calculated at any given point by obtaining the incident and reflected field using the γ_m and C_m of that mode. For this research work, a computer program was developed in the FORTRAN 90 to apply the MPM and least-squares fit to the MoM field samples.

In Chapter 3, the MPM was used to analyze various 2-D guiding structures. The structures were solved using the MoM and the MoM data was then used in the MPM. The MPM β was in excellent agreement with the theoretical wavenumber. It has been proved that the MPM along with the least-squares method can extract the γ_m and C_m from the MoM near-field data, and the extracted components can be used to reconstruct the original MoM near field. It also has been confirmed that as long as the sampling region is not too close to the open ends of the structures this approach

is reliable.

The reflection coefficient was calculated using the MPM γ_m and least squares C_m. For closed-end structures, it has been proved that this approach is perfect by comparing the calculated results with the theoretical results (obtained from the boundary conditions of PEC). For open-ended structures, it was found that the plane wave excitation is not good because it causes the contamination of the field inside due to the edge diffractions from the open ends. Thus to be able to avoid this contamination the load was needed to be closed from the effecting open end. The approach of using a Salisbury screen was found useful to close the load. The objective of the Salisbury screen was to absorb the incoming waves and hence to prevent the reflection from the closed end. We have confirmed that the absorber termination with Salisbury screen provides a remarkable improvement in the calculation of the reflection coefficient when the mode traveling in the structure is TEM.

In Chapter 4, a periodic 2-D LWA with plane wave excitation was solved by using the MoM. The field samples were taken by avoiding the open ends with a distance of $2\lambda_g$. The MPM extracted fast wave γ_m were in good agreement when compared with the SDMoM γ_m of 2-D strip grating. The MPM β_m were also in good agreement with the Floquet theory β_n. It has been demonstrated that the extracted γ_m and C_m associated with the fast waves can be used in the aperture integration to obtain the radiation pattern. The accuracy of this approach has been validated by comparisons with the aperture integration of the SDMoM γ_m and the radiation pattern from the reciprocity (MoM).

For practical situations, we can not just close the LWAs from the right end by putting a metal sheet, because then a strong beam will be present in the opposite direction, which is dependent on the reflected fast wave. But by leaving the end open, the edge diffractions from the incident plane wave cause the contamination of the field inside. A Salisbury screen was used to close the structures in the Chapter

3, which is suitable for TEM waves. More generally, if we close the structure, TM waves will hit the end with oblique angles of incidence, so a promising approach is to use an artificial absorber termination with Dallenbach layer, which absorbs the waves coming from a wide range of angles. It has been demonstrated that the Dallenbach absorber remarkably improves the reflection coefficient and the radiation pattern (by suppressing the forward beam).

Another periodic 2-D LWA (which is infinite in x and y) was considered for the MPM analysis. It was observed that the infinite and finite structures behave differently from one another when the plane wave excitation is used. The β changes by changing the plane wave angle of incidence. Therefore, further analysis of infinite structure was not done using this approach in this thesis.

In Chapter 5, a periodic 3-D LWA was analyzed using the MPM. The antenna was excited using an array of three magnetic dipoles near the origin inside the antenna. The objective of using an array was to approximate a uniform line source (TM_x polarization was assumed). The accuracy of the MPM extracted γ_m have been validated by comparisons with the Floquet theory β_n. It has also been verified that the extracted fast-wave component was getting more and more dominant as the height of the sampling region above the aperture was increasing, because the slow-wave component was getting weaker and weaker.

In the radiation pattern synthesis, the extracted fast wave γ_m and C_m were used in the aperture integration. A good agreement with the MoM radiation pattern was obtained by using just fast components. Some MPM extracted components with $\beta \approx k_0$, do not follow the Floquet theory. When they were used along with the fast wave components in the aperture integration, the radiation pattern was slightly changed. But the radiation pattern obtained from the fast-wave components was good enough to give a good agreement with the MoM radiation pattern. Therefore, these MPM extracted components (with $\beta \approx k_0$) were neglected for further analysis.

The reflection coefficient was calculated successfully using the extracted γ_m and C_m. This structure was excited by using a line source, which means the edge diffractions can not contaminate the field from open right end, and closed right end is not required. Therefore, the reflection coefficient Γ for 3-D LWA can be calculated without closing the structure. It has also been proved that finding the Γ for the radiating harmonics is a very useful tool for predicting the forward lobe of the LWA.

The effect of strip length on the behavior of 3-D LWA was also investigated. It was shown that by increasing the strip length of the LWA from $b = 5$ to 20 mm, the radiation pattern was changed. The new radiation pattern was very close to the 2-D LWA pattern. The MPM γ_m of the 3-D LWA with longer strips were in good agreement with the SDMoM γ_m of a 2-D strip grating. Eventually, it was demonstrated how the strip length affected the propagation constants, radiation pattern and reflection coefficient of LWA.

So far, the reflection coefficient was calculated using the fast wave components, but it was found challenging to make sense out of the reflection coefficient for the other components. In the near future, this problem would be solved. In 2-D analysis, more sources should be available to obtain the radiation pattern using the MoM. The plane wave excitation is not ideal, as it causes edge diffractions and also the radiation pattern can not be obtained for a transmitting antenna. In this thesis reciprocity was used to obtain the radiation pattern for a receiving antenna, which is an extremely slow procedure.

An infinitely long LWA could not be analyzed in detail because of the β dependency on the incident plane wave angle. It would be interesting if it is possible to analyze an infinite 2-D LWA using the MPM in order to obtain the correct space harmonics. It is hoped that this thesis might help other researchers in the future.

Bibliography

[1] W. Croswell and F. J. Zucker, "Surface-wave antennas," in *Antenna Engineering Handbook*, McGraw-Hill, New York, 2007.

[2] D. R. Jackson and A. A. Oliner, "Leaky-wave antennas," in *Modern Antenna Handbook*, John Wiley and Sons, 2008.

[3] C. Caloz, D. R. Jackson, and T. Itoh, "Leaky-wave antennas," in *Frontiers in Antennas: Next Generation Design and Engineering*, McGraw-Hill, New York, NY, Dec. 2011.

[4] A. A. Oliner and D. R. Jackson, "Leaky-wave antennas," in *Antenna Engineering Handbook* (J. Volakis, ed.), pp. 11.1–11.56, McGraw-Hill, 2007.

[5] W. W. Hansen, "Radiating electromagnetic waveguide," 1940. U.S. Patent No. 2,402,622.

[6] N. G. Alexopoulos and D. R. Jackson, "Fundamental superstrate (cover) effects on printed circuit antennas," *IEEE Trans. Antennas Propagat.*, vol. 32, pp. 807–816, August 1984.

[7] D. R. Jackson and N. G. Alexopoulos, "Gain enhancement methods for printed circuit antennas," *IEEE Trans. Antennas Propagat.*, vol. 33, pp. 976–987, Sept 1985.

[8] P. Feresidis and J. C. Vardaxoglou, "High gain planar antenna using optimized partially reflective surfaces," *IEEE Proc. Microwaves Antennas Propagat.*, vol. 148, pp. 345–350, Dec 2001.

[9] T. Zhao, D. Jackson, H. D. Yang, and A. A. Oliner, "2-d periodic leaky-wave antennas-part 1: metal patch design," *IEEE Trans. Antennas Propagat.*, vol. 53, p. 11, 2005.

[10] T. K. Sarkar and O. Pereira, "Using the matrix pencil method to estimate the parameters of a sum of complex exponentials," *IEEE Antennas and Propagation Magazine*, vol. 37, Feb 1995.

[11] F. R. Gantmachar, *Theory of Matrices*, vol. 1. New York, Chelsea, 1960.

[12] Y. Hua, *On techniques for estimating parameters of exponentially damped or undamped sinusoids in noise*. PhD thesis, Syracuse University, Syracuse, NY, 1988.

[13] T. K. Sarkar, R. S. Adve, and Z. A. Maricevic, "Utilization of the matrix pencil technique for determining the modal propagation characteristics of printed circuits," *Microwave symposium digest, IEEE MTT-S Inter.*, vol. 1, June 1996.

[14] Z. Altman, R. Mittra, O. Hashimoto, and E. Michielssen, "Efficient representation of induced currents on large scatterers using the generalized pencil of function method," *IEEE Trans. Antennas Propagat.*, vol. AP-7, pp. 51–57, 1996.

[15] C. D. Nallo, F. Mesa, and D. R. Jackson, "Excitation of leaky modes on multilayer stripline structures," *IEEE Trans. Microw. Theory Tech*, vol. 46, pp. 1062–1071, August 1998.

[16] Y.-C. Chen, C.-K. C. Tzuang, T. Itoh, and T. K. Sarkar, "Modal characteristics of planer transmission lines with periodical perturbations: Their behavior in

bound, stopband and radiation regions," *IEEE Trans. Antennas Propag.*, vol. 53, pp. 47–58, Jan 2005.

[17] A. K. Ozturk, *Vertex diffracted edge waves on a perfectly conducting plane angular sector*. PhD thesis, Concordia University, 2009.

[18] A. K. Ozturk and R. Paknys, "Analysis of propagation between rows of conducting cylinders that model solid surfaces using the same surface area rule," *IEEE Trans. Antennas Propagat.*, vol. 60, no. 5, 2012.

[19] FEKO user's manual 6.3. `http://www.feko.info`, 2013.

[20] Y. Hua and T. K. Sarkar, "Matrix pencil method of estimating parameters of exponentially damped/udamped sinusoid in noise," *IEEE Trans. Acoustic Speach Signal Processing*, vol. 38, pp. 834–844, May 2012.

[21] Y. Hua and T. K. Sarkar, "Generalized pencil-of-function method for extracting poles of an em system from its transient response," *IEEE Trans. on Antenna and Propagation*, vol. 37, February 1989.

[22] W. H. Press, B. P. Flannery, S. A. Teukolsky, and W.T.Vetterling, *Numerical Recipes*. Cambridge University Press, 1986.

[23] J. Dongarra, E. Grosse, *et al.*, "Netlib repository." `http://www.netlib.org`, c2000. Accessed: 2014-04-08.

[24] J. Encinar, "Mode-matching and point-matching techniques applied to the analysis of metal-strip-loaded dielectric antenna," *IEEE Trans. Antennas Propagat.*, vol. 38, pp. 1405–1412, Sep. 1990.

[25] T. Zhao, *Analysis and design of 2-D Periodic Leaky-Wave Antennas with metal patches or slots*. PhD thesis, University of Houston, 2003.

[26] E. F. Knott, J. Shaeffer, and M. T. Tuley, *Radar Cross Section*. SciTech Publishing, second ed., 2004.

[27] T. Ozdemir and J. L. Volakis, "A comparative study of an abc and an artificial absorber for truncating 3-d finite element meshes," *Antennas and Propagation Society International Symposium*, vol. 1, pp. 410–413, 1994.

[28] A. Singh, R. Paknys, and D. R. Jackson, "Using the matrix pencil method to analyze a 3d leaky wave antenna," *IEEE AP-S Symposium on Antenna and Propagation*, July 2015. Accepted.